Nonlinear Analysis: Hybrid Systems 45 (2022) 101192

Contents lists available at ScienceDirect

Nonlinear Analysis: Hybrid Systems

journal homepage: www.elsevier.com/locate/nahs

Stability and performance analysis of hybrid integrator–gain systems: A linear matrix inequality approach

Sebastiaan van den Eijnden *, W.P.M.H. Heemels, Henk Nijmeijer, Marcel Heertjes

Department of Mechanical Engineering, Eindhoven University of Technology, Eindhoven 5600 MB, The Netherlands

ARTICLE INFO

Article history:
Received 7 July 2021
Received in revised form 31 December 2021
Accepted 2 March 2022
Available online xxxx

Keywords:
Hybrid integrator–gain system
Linear matrix inequality (LMI)
$\mathcal{L}_2$-gain
$\mathcal{H}_2$-norm

ABSTRACT

Hybrid integrator–gain systems (HIGS) are nonlinear elements designed for overcoming fundamental limitations of linear time-invariant integrators. This paper presents numerically robust conditions for time-domain stability and performance of HIGS-controlled systems. In particular, using piecewise quadratic (PWQ) Lyapunov functions defined over polyhedral subregions of the state-space, conditions for stability and computations of upper-bounds on the $\mathcal{L}_2$-gain and $\mathcal{H}_2$-norm are formulated as convex optimization problems in terms of numerically tractable linear matrix inequalities (LMIs). In order to improve accuracy and robustness, the LMIs are constructed in a manner to eliminate explicit equality constraints typically related to continuity of the PWQ functions. Novel conditions are presented that guide further refinement of the subregions over which the PWQ Lyapunov functions are defined in order to increase the accuracy of the approach. The effectiveness of the presented analysis tools is demonstrated through a numerical case-study on a motion system.

1. Introduction

The widespread use of linear time-invariant (LTI) control in industry is often attributed to its simplicity of design and predictability of performance. However, in view of the ever increasing demands on precision and throughput of high-performance systems such as wafer scanners, pick-and-place machines, and industrial printers, the classical trade-offs encountered when using LTI control are becoming performance-limiting factors [1,2].

Nonlinear control systems potentially deal with these trade-offs in a different manner, and may therefore provide a means to realize performance that is unattainable by any linear design [3,4]. From a motion control perspective, nonlinear strategies that aim at resembling the behaviour of linear filters such as integrators, while improving upon the negative effects of the associated phase lag, are of particular interest. Typical examples in this regard include split-path nonlinear (SPAN) integrators [5,6], switching control [7,8], reset integrators [9–19], and the recently introduced hybrid integrator–gain system (HIGS) [20,21]. The main philosophy of the latter two nonlinear integrators is quite comparable: whenever appropriate algebraic conditions on the input–output pair are satisfied, the integrator buffer is emptied, either instantaneously as with reset control or gradually as with HIGS, thereby forcing the input–output signals to have equivalent signs. The potential benefits can be made visible amongst others from a describing function analysis. For reset control elements as well as for HIGS it is found that the magnitude of the dominant harmonic in the response

* Corresponding author.
E-mail addresses: s.j.a.m.v.d.eijnden@tue.nl (S. van den Eijnden), m.heemels@tue.nl (W.P.M.H. Heemels), h.nijmeijer@tue.nl (H. Nijmeijer), m.f.heertjes@tue.nl (M. Heertjes).

https://doi.org/10.1016/j.nahs.2022.101192

to a sinusoidal input shows a 20 dB/decade amplitude decay, similar to a linear integrator, but with an associated phase lag that does not exceed 38.15 degrees, see [9,22]. This defies Bode's gain–phase relationship for linear systems and hints toward the possibility for performance improvements. The main difference between reset control and HIGS, however, is that reset control achieves this phase advantage in its describing function by means of discontinuous outputs, whereas HIGS generates continuous (though non-smooth) outputs. The latter could be beneficial from both a theoretical as well as a practical point-of-view. Let us also motivate the differences between HIGS-based control and the switched controller design approach in [7], where a family of LTI controller realizations is constructed that yield a stable closed-loop system when switching *arbitrarily* between them. In that work, stability of each of the LTI subsystems is required. Distinctively, HIGS employs a specific state-based switching strategy that allows for the underlying subsystems to be unstable, thereby making it fundamentally different from the framework discussed in [7]. Switching between one (or more) unstable modes is, in fact, believed to be a key contributor to improved system performance with HIGS as will be shown in a numerical example presented in this paper. Experimental studies on an industrial wafer scanner in [20,22,23] have demonstrated the practical potential of HIGS, and recently it has been shown in [24] that HIGS can truly overcome fundamental limitations of LTI control, further supporting its relevance and potential.

This paper is concerned with systematic stability and performance analysis of HIGS-controlled systems. In particular, rigorous conditions for verifying time-domain stability and performance are presented. These conditions are based on finding suitable continuous *piecewise* quadratic (PWQ) functions by solving sets of LMIs. The motivation for considering PWQ functions comes from their success in reducing conservatism in the analysis of piecewise linear systems, see for example the seminal works in [25,26]. The use of PWQ functions for system analysis has been successfully applied to numerous fields of applications, including reset control [12,14,16]. For HIGS-controlled systems, this approach was pioneered in [21,27]. In these works, the three-dimensional subspace determining the active dynamics of HIGS is partitioned into polyhedral regions, each to which a local Lyapunov-like function is assigned. Continuity of the functions over a shared region boundary is guaranteed by posing explicit equality constraints. From a computational point-of-view, however, such constraints are particularly hard to satisfy since numerical solvers work with finite precision and can therefore only approximate a solution. A result that most likely violates the equality constraints is returned, potentially leading to false conclusions on stability [28]. In order to slightly relax the conditions, a small mismatch on the boundary plane between two successive functions can be allowed [16]. However, choosing an acceptable mismatch is not straightforward: too small may yield infeasible results, whereas too large can easily result in false conclusions.

The main objective in this paper is to improve upon the stability and performance analysis results presented in [21] from both a theoretical as well as a numerical point-of-view. In doing so, inspiration is drawn from the work in [25,26] where a compact matrix parametrization of piecewise quadratic functions on polyhedral partitions is introduced. This parametrization allows for the continuity requirement to be directly incorporated in the description of each local Lyapunov-like function. In order to pursue this approach for HIGS-controlled systems, a specific partitioning of HIGS' input–output space is proposed that allows for systematic construction of the key matrix parametrization, thereby guaranteeing continuity a priori, and making the need for equality constraints in the eventual set of LMIs redundant. Moreover, such partitioning strategy provides additional flexibility over the existing polyhedral strategy in [21], since polyhedral partitions can always be recovered with a simplicial partition, but not vice versa. This positively contributes to an increased accuracy of the presented conditions for stability and performance.

In line with the above, the paper presents two main contributions. First, rigorous conditions for evaluating stability and performance of hybrid integrator–gain systems are presented. Performance is expressed in terms of both the $\mathcal{L}_2$-gain, and the $\mathcal{H}_2$-norm [29]. By exploiting piecewise quadratic Lyapunov functions with a tailored simplicial partitioning, the conditions are formulated as LMIs in a manner that is flexible, systematic, and robust from a numerical perspective. From a theoretical perspective, the approach does not introduce conservatism as compared to the approach in [21], but, in fact, increases the class of admissible Lyapunov functions. As a second contribution, novel algebraic conditions are presented that provide relevant insights regarding (in)feasibility of the LMIs. These results rigorously demonstrate the benefits obtained from exploiting partition refinements, and help in guiding such refinements as to increase the possibility of finding a solution to the presented LMI conditions. To the best of the authors knowledge, algebraic results formally demonstrating the benefits of partition refinement have not been presented in the literature before. The effectiveness of the presented tools is demonstrated in an extensive numerical case study.

The remainder of the paper is organized as follows. Section 2 contains notations and definitions that are used throughout this paper. In Section 3, HIGS is introduced and its use for feedback control is discussed. In Section 4, time-domain stability and performance conditions based on PWQ functions are presented in the form of LMIs along with some necessary conditions for their feasibility. Applicability of the presented analysis tools is demonstrated through a numerical example in Section 5. Section 6 presents the main conclusions.

2. Notation and definitions

In this paper, the set of real symmetric matrices in $\mathbb{R}^{n\times n}$ is denoted by $\mathbb{S}^{n\times n}$, and the set of real symmetric matrices having non-negative elements is denoted by $\mathbb{S}^{n\times n}_{\geq 0}$. The inequality symbols $>, \geq, <, \leq$ for vectors are understood componentwise. The interior of a set $\mathcal{X}$ is denoted by $\operatorname{int}(\mathcal{X})$ and the closure by $\overline{\mathcal{X}}$. For a signal $t \mapsto x(t)$, the notation $\operatorname{dom} x$ denotes its projection on the time (t) axis, and $T = \sup \operatorname{dom} x$ indicates the maximal time of the domain.

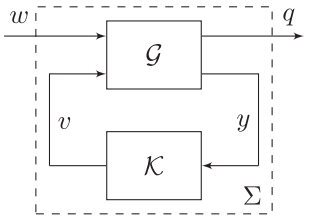

Fig. 1. Generalized plant interconnection Σ.

Definition 1 (*Positive Hull, [30]*)**.** The positive hull of a set $\mathcal{R} \subset \mathbb{R}^n$ is the set of all positive combinations of elements from $\mathcal{R}$, i.e.,

$$\operatorname{pos}(\mathcal{R}) = \left\{ \sum_{m=1}^{M} \lambda_m r_m \mid r_m \in \mathcal{R}, \lambda_m \geq 0, M \in \mathbb{N}_{>0} \right\}.$$

Definition 2 (*Polyhedral Cone, [30]*)**.** A polyhedral cone is the positive hull of a set $\mathcal{R} := \{r_1, \ldots, r_M\}$ with a finite number of elements. In this case $\mathcal{R}$ is called the generating set of the polyhedral cone, and $r_1, \ldots, r_M$ are generators.

Definition 3 (*Simplicial Cone, [30]*)**.** A simplicial cone in $\mathbb{R}^n$ is the positive hull of a set $\mathcal{R}$ with n linearly independent generators.

Polyhedral and simplicial cones can be written as

$$\mathcal{C} = \left\{ x \in \mathbb{R}^n \mid Cx \geq 0 \right\},$$

for some suitable matrix $C \in \mathbb{R}^{q \times n}$ of full rank. For simplicial cones it follows that C is a square invertible matrix. The notation $-\mathcal{C}$ indicates the set $\{x \in \mathbb{R}^n \mid -x \in \mathcal{C}\}$. For a more detailed discussion on polyhedral and simplicial cones, the reader is referred to, *e.g.,* [30, Chapter 1].

Definition 4 (*Simplicial Partition, [31]*)**.** Let a set $\mathcal{F} \subseteq \mathbb{R}^n$ and an integer $N > 0$ be given. A simplicial partition of $\mathcal{F}$ is a family $\mathcal{S} = \{\mathcal{C}_1, \ldots, \mathcal{C}_N\}$ consisting of a finite number of simplicial cones $\mathcal{C}_i$, $i \in \mathcal{N} := \{1, \ldots, N\}$ that satisfy $\mathcal{F} = \bigcup_{i \in \mathcal{N}} \mathcal{C}_i$, and $\operatorname{int}(\mathcal{C}_i) \cap \operatorname{int}(\mathcal{C}_j) = \emptyset$ for $i \neq j$.

3. Control context and system description

The results presented in this paper involve the general control configuration as depicted in Fig. 1. Here, $\mathcal{G}$ is the generalized plant, which is represented as the linear time-invariant (LTI) multi-input multi-output (MIMO) system

$$\mathcal{G} : \begin{pmatrix} q \\ y \end{pmatrix} = \begin{pmatrix} \mathcal{G}_{11} & \mathcal{G}_{12} \\ \mathcal{G}_{21} & \mathcal{G}_{22} \end{pmatrix} \begin{pmatrix} w \\ v \end{pmatrix}, \tag{1}$$

where $q(t) \in \mathbb{R}^m$ contains the performance variables, which typically include tracking errors and control actions, and $w(t) \in \mathbb{R}^n$ contains the exogenous variables, such as disturbances, noise, and reference profiles at time $t \in \mathbb{R}_{\geq 0}$. The controller input and output are denoted by $y(t) \in \mathbb{R}$, and $v(t) \in \mathbb{R}$, respectively, and $\mathcal{G}_{ij}(s)$, $s \in \mathbb{C}$, $i, j \in \{1, 2\}$, are transfer function matrices of appropriate dimensions.

Typically, $\mathcal{G}$ contains the physical plant to be controlled, possibly augmented with LTI input- and output weighting filters. These filters are added for the purpose of including problem specific input knowledge into the system description, *e.g.*, through known spectra of exogeneous signals, and penalizing regulated output variables. The use of weighting filters is standard practice in H_∞-design problems, see [32].

The generic structure of the single-input single-output (SISO) HIGS-based controller $\mathcal{K}$ is shown in Fig. 2, and is regarded as the interconnection of the hybrid integrator–gain system $\mathcal{H}$, specified in more detail in Section 3.1 below, and an LTI MIMO system $\mathcal{C}$, the latter given by

$$\mathcal{C} : \begin{pmatrix} v \\ z \end{pmatrix} = \begin{pmatrix} \mathcal{C}_{11} & \mathcal{C}_{12} \\ \mathcal{C}_{21} & \mathcal{C}_{22} \end{pmatrix} \begin{pmatrix} y \\ u \end{pmatrix}, \tag{2}$$

in which $\mathcal{C}_{ij}(s) \in \mathbb{C}$, $i, j \in \{1, 2\}$, are transfer functions associated with the LTI filters, and $z(t), u(t) \in \mathbb{R}$ denote the input and output to the HIGS, respectively.

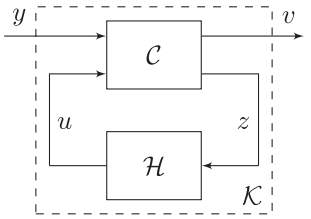

Fig. 2. Generic structure of the HIGS-based controller $\mathcal{K}$.

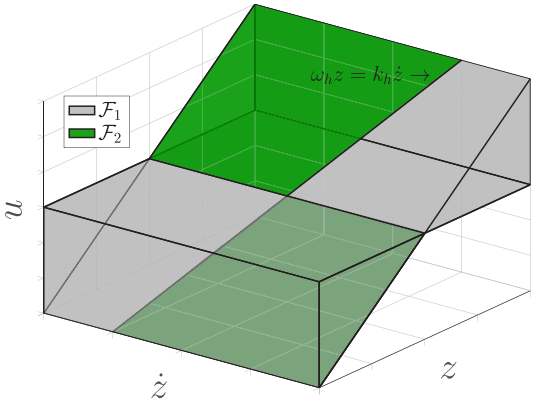

Fig. 3. Three-dimensional region $\mathcal{F}$ defined in (4) which determines the active dynamics of HIGS. Here, $\mathcal{F}_1$ (grey) defines the integrator-mode region, and $\mathcal{F}_2$ (green) the gain-mode region. (For interpretation of the references to colour in this figure legend, the reader is referred to the web version of this article.)

3.1. Hybrid Integrator–Gain System (HIGS)

The HIGS has been mathematically formulated in several ways. For instance in [20], it was presented as a discontinuous piecewise linear (PWL) system, whereas more recently in [21,33] it is formally introduced and modelled in terms of the extended projected dynamical system (ePDS) framework, which is closer and more natural to the engineering philosophy behind HIGS. In the latter work it is shown that said representations are equivalent. Throughout the rest of this paper, the PWL system formulation is adopted as this one is more convenient for the analysis purposes in this paper. In particular, the HIGS is represented as the PWL system with discontinuous right-hand side given by

$$\mathcal{H}: \begin{cases} \dot{x}_h = \omega_h z & \text{if } (z,u,\dot{z}) \in \mathcal{F}_1, \\ x_h = k_h z & \text{if } (z,u,\dot{z}) \in \mathcal{F}_2, \\ u = x_h, \end{cases} \tag{3}$$

where $x_h(t) \in \mathbb{R}$ denotes the state of the integrator, $z(t) \in \mathbb{R}$ is the input, which is assumed to be of class C^1, $\dot{z}(t) \in \mathbb{R}$ is the corresponding time-derivative, and $u(t) \in \mathbb{R}$ is the generated output. The parameter $\omega_h \in \mathbb{R}_{>0}$ is the integrator frequency, and $k_h \in \mathbb{R}_{>0}$ is the gain. In (3), the sets $\mathcal{F}_1$ and $\mathcal{F}_2$ denote subregions of $\mathbb{R}^3$ in which HIGS represents (i) an integrator or (ii) a gain, respectively. By design, the union of these sets is given by

$$\mathcal{F} := \mathcal{F}_1 \cup \mathcal{F}_2 = \left\{(z,u,\dot{z}) \in \mathbb{R}^3 \mid k_h z u \geq u^2\right\}, \tag{4}$$

which confines the input–output relation of the HIGS to the $[0, k_h]$-sector. As motivated in [20–22], it is intended for the HIGS to primarily exhibit integrator dynamics. Therefore, the region $\mathcal{F}_1$ is maximized in such a way that a switch from 'integrator mode' to 'gain mode' is invoked only when the $(z,u,\dot{z})$-trajectory tends to escape the sector $\mathcal{F}$ in integrator-mode. This results in the following definitions for $\mathcal{F}_1$ and $\mathcal{F}_2$:

$$\mathcal{F}_1 := \mathcal{F} \setminus \mathcal{F}_2, \tag{5a}$$

$$\mathcal{F}_2 := \left\{(z,u,\dot{z}) \in \mathcal{F} \mid u = k_h z \wedge \omega_h z^2 > k_h \dot{z} z\right\}, \tag{5b}$$

where $\mathcal{F}_2$ defines a sector on a lower-dimensional space in $\mathcal{F}$ with measure zero (in the sense of Lebesgue). The set $\mathcal{F}$, and corresponding subsets $\mathcal{F}_1$ and $\mathcal{F}_2$ are visualized in Fig. 3. In fact, the gain-dynamics can be seen as a (partial) projection of the integrator dynamics on the sector $\mathcal{F}$, see [21,33] for more details on this perspective of projected dynamical systems.

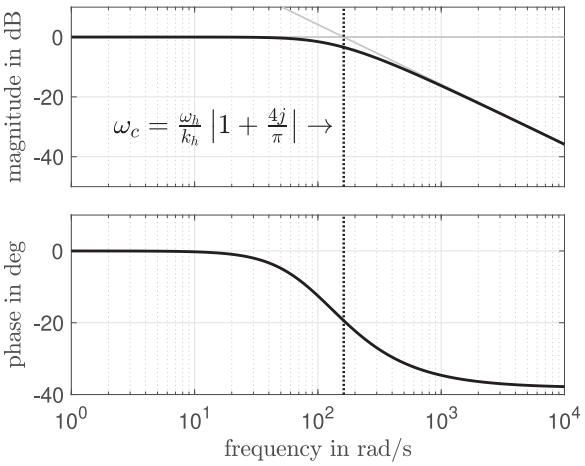

Fig. 4. Describing function of the HIGS (6) with cross-over frequency $\omega_c = \omega_h|1 + 4j/\pi|/k_h$ rad/s.

In frequency-domain, the properties of HIGS in (3) can be studied (to some extent) by its describing function $\mathcal{D}(j\omega) \in \mathbb{C}$, *i.e.*, the complex mapping from a sinusoidal input $z(t) = \sin(\omega t)$ to the first harmonic in the corresponding output $u(t)$. In [22] this mapping has been derived analytically as

$$\mathcal{D}(j\omega) = \frac{\omega_h}{j\omega}\left(\frac{\gamma}{\pi} + j\frac{e^{-2j\gamma}-1}{2\pi} - 4j\frac{e^{-j\gamma}-1}{2\pi}\right) + k_h\left(\frac{\pi-\gamma}{\pi} + j\frac{e^{-2j\gamma}-1}{2\pi}\right), \tag{6}$$

with $\gamma = 2\arctan(k_h\omega/\omega_h) \in [0, \pi]$. A Bode-like representation of the describing function (6) is depicted in Fig. 4, and demonstrates first-order low-pass magnitude characteristics, with an induced phase lag of 38.15 degrees at most. Specific use of HIGS for improving the phase characteristics of LTI filters based on describing function reasoning can be found in, *e.g.*, [22–24,27].

3.2. Closed-loop system description

The linear portion of the closed-loop system in Fig. 1, resulting from the feedback interconnection of the plant $\mathcal{G}$ in (1) with $\mathcal{C}$ in (2), is given by

$$\Sigma_{\text{lin}} : \begin{cases} \dot{x}_l &= A_l x_l + B_l w + B_u u, \\ q &= C_l x_l + D_l w + D_u u, \\ z &= C_z x_l + D_w w + D_z u, \end{cases} \tag{7}$$

with states $x_l(t) \in \mathbb{R}^p$, input $u(t) \in \mathbb{R}$ generated by HIGS, external inputs $w(t) \in \mathbb{R}^n$, and performance output $q(t) \in \mathbb{R}^m$, at time $t \in \mathbb{R}_{\geq 0}$. The output $z(t) \in \mathbb{R}$ is used as input to the HIGS in (3). Conform Figs. 1 and 2, the system matrices in (7) satisfy (where for the sake of brevity dependency on s is omitted)

$$\begin{aligned} \Sigma_{qu}(s) &= C_l\,(sI - A_l)^{-1}\,B_u + D_u \\ &= \mathcal{G}_{12}\,(I - \mathcal{C}_{11}\mathcal{G}_{22})^{-1}\,\mathcal{C}_{12}, \end{aligned} \tag{8}$$

$$\begin{aligned} \Sigma_{qw}(s) &= C_l\,(sI - A_l)^{-1}\,B_l + D_l \\ &= \mathcal{G}_{11} + \mathcal{G}_{12}\,(I - \mathcal{C}_{11}\mathcal{G}_{22})^{-1}\,\mathcal{C}_{11}\mathcal{G}_{21}, \end{aligned} \tag{9}$$

which denote the transfers from u to q, and w to q, respectively, and

$$\begin{aligned} \Sigma_{zu}(s) &= C_z\,(sI - A_l)^{-1}\,B_u + D_z \\ &= \mathcal{C}_{22} + \mathcal{C}_{21}\mathcal{G}_{22}\,(I - \mathcal{C}_{11}\mathcal{G}_{22})^{-1}\,\mathcal{C}_{12}, \end{aligned} \tag{10}$$

$$\begin{aligned} \Sigma_{zw}(s) &= C_z\,(sI - A_l)^{-1}\,B_l + D_w \\ &= \mathcal{C}_{21}\big(I + \mathcal{G}_{22}\,(I - \mathcal{C}_{11}\mathcal{G}_{22})^{-1}\,\mathcal{C}_{11}\big)G_{21}, \end{aligned} \tag{11}$$

being the transfer functions from u to z, and w to z, respectively. To ensure that the interconnected system resulting from the linear system (7) with HIGS is well-posed, the following assumption is made, see [21] for a formal discussion.

Assumption 1. The transfer functions $\Sigma_{zu}(s)$ in (10) and $\Sigma_{zw}(s)$ in (11) have a relative degree of at least two, i.e., $D_z = D_w = 0$ and $C_z B_l = C_z B_u = 0$.

The assumption on $\Sigma_{zu}(s)$ removes the occurrence of an algebraic loop when HIGS is in gain-mode, whereas the assumption on $\Sigma_{zw}(s)$ results in the absence of a direct feedthrough from the signals $(w, \dot{w})$ to $(z, \dot{z})$. The latter will prove useful for system analysis. Note that the relevant and broad class of motion systems typically satisfy Assumption 1. Moreover, it directly reflects the filtering hypothesis [34] that is usually made for justifying the use of describing functions, as the transfer from the output of HIGS to its input, which is governed by $\Sigma_{zu}(s)$, has certain low-pass filtering characteristics.

The closed-loop interconnection of (7) with HIGS in (3) then naturally admits the PWL representation

$$\Sigma : \begin{cases} \dot{x} &= A_i x + Bw, \quad \text{if } Hx \in \mathcal{F}_i,\ i \in \{1, 2\} \\ q &= Cx + Dw \end{cases} \tag{12}$$

with state vector $x(t) = \left[x_l(t)^\top\ x_h(t)\right]^\top \in \mathbb{R}^{p+1}$, and performance outputs $q(t) \in \mathbb{R}^m$. The matrix H extracts those signals from x that determine mode switching of HIGS, *i.e.*, H is such that $Hx := [z\ u\ \dot{z}]^\top$, and is, therefore, given by

$$H^\top = \begin{bmatrix} C_z^\top & 0 & (C_z A_l)^\top \\ 0 & 1 & 0 \end{bmatrix}. \tag{13}$$

The (mode-dependent) system matrices are given by

$$\left[\begin{array}{c|c} A_i & B \\ \hline C & D \end{array}\right] = \left[\begin{array}{cc|c} A_l & B_u & B_l \\ A_{h,i} & 0 & 0 \\ \hline C_l & D_u & D_l \end{array}\right], \tag{14}$$

with $A_{h,1} = \omega_h C_z$ and $A_{h,2} = k_h C_z A_l$. Note that the system matrices in gain mode ($i = 2$) result from explicit differentiation of the algebraic constraint $x_h = k_h z$ in (3). In this regard, it is worth mentioning that the system described in (12) is conceptually different from the systems treated in, *e.g.*, [25,26], as part of the dynamics evolve on a lower-dimensional manifold and the dynamics are discontinuous. Note also that [26] considers piecewise continuously differentiable solutions, while in this paper absolutely continuous solutions are allowed. Care is needed to deal with the discontinuous nature of the dynamics and corresponding solutions, see, *e.g.*, [35]. The discontinuous nature of the dynamics renders the existence of solutions not immediate. However, in [21,33] it has been shown that for inputs w belonging to the class of piecewise Bohl functions [21, Definition 2], forward completeness of solutions to (12) is formally guaranteed. It is stressed that further improvements on well-posedness properties of the system in (12) are beyond the scope of this paper.

4. Time-domain analysis

In this section, sufficient conditions for stability and performance, the latter characterized in terms of the $\mathcal{L}_2$-gain and the $\mathcal{H}_2$-norm, of the closed-loop system in (12) are presented. The conditions are preferred to be computationally tractable, and flexible. For that purpose, an approach, which is inspired by the works in [14,21], and exploits piecewise quadratic (PWQ) functions is pursued.

4.1. Partition strategy and constraint matrices

Key in the construction of general PWQ functions is the division of (a subset of) the state-space of the considered system into smaller sub-regions. In order to guarantee continuity of the PWQ functions over a boundary shared by two adjacent regions, different approaches exist. In [14,21], continuity conditions are posed in the form of explicit equality constraints, whereas in [25] the continuity property is directly incorporated in the construction of the PWQ function. Particularly, in [25] a compact matrix parametrization of piecewise quadratic functions on polyhedral partitions is introduced as

$$V_i(x) = x^\top P_i x = x^\top F_i^\top \Phi F_i x, \tag{15}$$

where $F_i \in \mathbb{R}^{r \times n}$ form the so-called *continuity matrices* satisfying $F_i x = F_j x$ for all x on a boundary shared by two polyhedral regions, and $\Phi \in \mathbb{S}^{r \times r}$ is a symmetric matrix that contains the decision variables. By construction, continuity of the PWQ functions over cell boundaries is guaranteed (see Lemma 4.2 in [25]), thereby making the equality constraints obsolete. Note that from a numerical perspective this is considered a major benefit, as equality constraints are typically hard to solve exactly, thereby potentially compromising the stability and performance certificates [28]. Construction of appropriate continuity matrices in (15) depends on the considered partitioning, and may be quite involved (if at all possible), for example in the case of *polyhedral* partitions such as the one proposed for the HIGS in [21]. However, for *simplicial* partitions (see Definition 4), constructing the continuity matrices can be done in an efficient manner, as will be shown. Moreover, as each polyhedral region can be partitioned into a finite number of simplicial regions [30, Lemma 1.40], a piecewise function defined over polyhedral regions can equivalently be described over simplicial regions (albeit with more regional descriptions) but not vice versa. Hence, a simplicial partitioning provides additional flexibility that may increase the class of admissible Lyapunov functions, and in that sense increases the accuracy in the analysis as compared to, for example, the approach in [21].

Motivated by the preceding discussion and for the sake of (computational) improvement, a simplicial partition of the three-dimensional region $\mathcal{F}$ is proposed. From (4) and Fig. 3 it can be seen that the set $\mathcal{F}$ is formed as the union of two polyhedral cones $\mathcal{K}$ and $-\mathcal{K}$, that is,

$$\mathcal{F} = \underbrace{\left\{\xi \in \mathbb{R}^3 \mid K\xi \geq 0\right\}}_{:=\mathcal{K}} \cup \underbrace{\left\{\xi \in \mathbb{R}^3 \mid K\xi \leq 0\right\}}_{:=-\mathcal{K}}. \tag{16}$$

where $\xi = [z, u, \dot{z}]^\top = Hx$, and

$$K = \begin{bmatrix} 0 & 1 & 0 \\ k_h & -1 & 0 \end{bmatrix}. \tag{17}$$

The intersection of $\mathcal{K}$ and $-\mathcal{K}$ is defined by $K\xi = 0$, and coincides with the line $\xi = \left\{[0, 0, \dot{z}]^\top \mid \dot{z} \in \mathbb{R}\right\}$. According to [30, Lemma 1.40], polyhedral cones with nonempty interior can always be partitioned into a finite number of simplicial cones. This result allows the polyhedral cone $\mathcal{K}$ in (16) to be partitioned into N simplicial cones $\mathcal{S}_i$ given by

$$\mathcal{S}_i = \left\{\xi \in \mathbb{R}^3 \mid S_i\xi \geq 0\right\}. \tag{18}$$

Let the simplicial partition of $\mathcal{K}$ be denoted by

$$\mathcal{S}_\mathcal{K} := \{\mathcal{S}_1, \ldots, \mathcal{S}_N\}, \tag{19}$$

and consider the index set $\mathcal{N} := \{1, \ldots, N\}$. A generating set $\mathcal{R}_\mathcal{S}$ of the partition $\mathcal{S}_\mathcal{K}$ is constructed as the union of generating sets $\mathcal{R}_i^\mathcal{S}$ of each simplicial cone $\mathcal{S}_i \in \mathcal{S}_\mathcal{K}$, *i.e.*, $\mathcal{R}_\mathcal{S} = \bigcup_{i\in\mathcal{N}} \mathcal{R}_i^\mathcal{S}$. In what follows, it is assumed that the simplicial partition $\mathcal{S}_\mathcal{K}$ is constructed in such a manner that the vectors $[0, 0, 1]^\top$ and $[0, 0, -1]^\top$ are generators, and thus $[0, 0, \pm 1]^\top \in \mathcal{R}_\mathcal{S}$. Note that due to symmetry, a partitioning of $-\mathcal{K}$ directly results from a partitioning of $\mathcal{K}$, and is denoted by $-\mathcal{S}_\mathcal{K}$. A simplicial partition of $\mathcal{F}$ is then given by $\mathcal{S} := \mathcal{S}_\mathcal{K} \cup -\mathcal{S}_\mathcal{K}$. In turn, since $\overline{\mathcal{F}}_1 = \mathcal{F}$, a partition of $\mathcal{F}_1$ is equivalent to a partition of $\mathcal{F}$, and, therefore, is given by $\mathcal{S}$, whereas a partition of $\mathcal{F}_2$ is formed by M boundary faces of $\mathcal{S}$. In particular, these boundary faces are described by $\mathcal{T}_j = \text{pos}\left\{r_k^m, r_k^n\right\}, j \in \mathcal{M} := \{1, \ldots, M\}$, for some $k \in \mathcal{N}$ and $(m, n) \in \{1, 2, 3\}^2$. Here, r_k^m, r_k^n are generators of $\mathcal{S}_k$ that satisfy $r_k^m, r_k^n \in \overline{\mathcal{F}}_2$. The generating set of $\mathcal{T}_j$ is given by $\mathcal{R}_j^\mathcal{T} = \left\{r_k^m, r_k^n\right\}$. Clearly, $\mathcal{T}_j$ are polyhedral cones in $\mathbb{R}^3$ and can alternatively be described by

$$\mathcal{T}_j = \left\{\xi \in \mathbb{R}^3 \mid T_j\xi \geq 0 \wedge \Pi\xi = 0\right\}, \tag{20}$$

where $T_j \in \mathbb{R}^{2\times 3}$ is a full row rank matrix, $j \in \mathcal{M}$, and $\Pi := [k_h, -1, 0]$. Denote the partition of the gain-mode subset $\mathcal{F}_2$ by $\mathcal{T}$ and observe that

$$\mathcal{T} := \underbrace{\{\mathcal{T}_1, \ldots, \mathcal{T}_M\}}_{:=\mathcal{T}_\mathcal{K}} \cup \underbrace{\{-\mathcal{T}_1, \ldots, -\mathcal{T}_M\}}_{:=-\mathcal{T}_\mathcal{K}}. \tag{21}$$

The generating set $\mathcal{R}_\mathcal{T}$ of the partition $\mathcal{T}_\mathcal{K}$ is formed as $\mathcal{R}_\mathcal{T} := \bigcup_{j\in\mathcal{M}} \mathcal{R}_j^\mathcal{T}$, and contains all generators r of $\mathcal{S}$ that satisfy $r \in \overline{\mathcal{F}}_2$. A possible partition of $\mathcal{F}$ into simplicial cones is illustrated in Fig. 5. Several efficient numerical procedures can be employed for constructing an appropriate simplicial division of an n-dimensional space, such as bisection along the longest edge techniques [31], and ray-gridding algorithms [36].

One of the main advantages of the partitioning strategy as illustrated in Fig. 5, is the possibility for easy and systematic construction of the matrices S_i, T_j in (18) and (20), and the continuity matrices F_i in (15). The former matrices are used in the upcoming analysis for the construction of S-procedure relaxation terms. The following two propositions present results for the construction of appropriate matrices associated with a simplicial partitioning of the HIGS' sector $\mathcal{F}$. These are based on the ideas outlined in the seminal works [26] and [25, Chapter 8, Section 8.1].

Proposition 1. *Consider a simplicial partition $\mathcal{S}$ of $\mathcal{F}$. Collect the generators of each simplicial cone $\mathcal{S}_i \in \mathcal{S}$ in a matrix $R_i := \left[r_1^i, r_2^i, r_3^i\right] \in \mathbb{R}^{3\times 3}$, $i \in \mathcal{N}$, and the generators of $\mathcal{T}_j \in \mathcal{T}$, $j \in \mathcal{M}$, in a matrix $\hat{R}_j := [r_1^j, r_2^j] \in \mathbb{R}^{3\times 2}$. Then the matrices*

$$S_i = R_i^{-1}, \qquad i \in \mathcal{N} \tag{22}$$

$$T_j = \left(\hat{R}_j^\top \hat{R}_j\right)^{-1} \hat{R}_j^\top, \qquad j \in \mathcal{M} \tag{23}$$

and $\Pi = [k_h, -1, 0]$ satisfy the inequalities specified in (18) and (20), respectively.

Proof. First, it is shown that $\xi \in \mathcal{S}_i \iff S_i\xi \geq 0$.

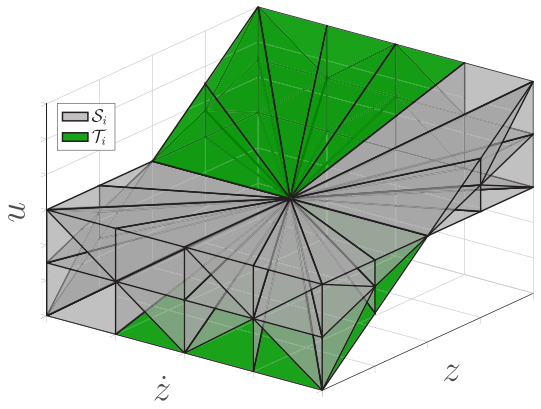

Fig. 5. Simplicial partition of $\mathcal{F}$. Each three-dimensional simplicial cone $\mathcal{S}_i$ (grey shaded) is spanned by three vectors r_i^1, r_i^2, r_i^3, *i.e.*, $\mathcal{S}_i = \text{pos}\left\{r_i^1, r_i^2, r_i^3\right\}$. The green shaded regions correspond to boundary faces $\mathcal{T}_j$ that partition the gain-mode region. (For interpretation of the references to colour in this figure legend, the reader is referred to the web version of this article.)

- $\xi \in \mathcal{S}_i \Rightarrow S_i\xi \geq 0$. Since $\mathcal{S}_i$ is a simplicial cone, each $\xi \in \mathcal{S}_i$ can uniquely be written as a positive combination of columns from R_i, *i.e.*,

$$\xi = R_i\lambda, \text{ with } 0 \leq \lambda \in \mathbb{R}^3. \tag{24}$$

  Invertibility of R_i results in $\lambda = R_i^{-1}\xi \geq 0$, which by the choice $S_i = R_i^{-1}$ yields the inequality.
- $S_i\xi \geq 0 \Rightarrow \xi \in \mathcal{S}_i$. Suppose $S_i\xi = \lambda \geq 0$. Invertibility of S_i yields $\xi = R_i\lambda$ and thus $\xi \in \text{pos}\left\{r_i^1, r_i^2, r_i^3\right\} = \mathcal{S}_i$. The result follows.

Next it is shown that $\xi \in \mathcal{T}_i \Longleftrightarrow T_i\xi \geq 0, \Pi\xi = 0$.

- $\xi \in \mathcal{T}_j \Rightarrow T_j\xi \geq 0, \Pi\xi = 0$. The equality follows immediately from the observation that $\mathcal{T}_j \subset \mathcal{F}_2$. Since $\mathcal{T}_j$ is a polyhedral cone, each $\xi \in \mathcal{T}_j$ can be written as the positive combination of columns in $\hat{R}_j$, that is

$$\xi = \hat{R}_j\lambda, \text{ with } 0 \leq \lambda \in \mathbb{R}^2. \tag{25}$$

  Since $\hat{R}_j$ has linearly independent columns, it follows that the matrix product $\hat{R}_j^\top\hat{R}_j$ also has linearly independent columns and, therefore, is invertible. Multiplying (25) from the left by $(\hat{R}_j^\top\hat{R}_j)^{-1}\hat{R}_j^\top$ yields

$$\left(\hat{R}_j^\top\hat{R}_j\right)^{-1}\hat{R}_j^\top\xi = \lambda \geq 0.$$

  From the choice for T_j in (23) the result follows.
- $T_j\xi \geq 0, \Pi\xi = 0 \Rightarrow \xi \in \mathcal{T}_j$. Suppose $T_j\xi = \lambda$ with $\lambda \geq 0$. Pre-multiplication of this equality with $\hat{R}_j^\top\hat{R}_j$ yields $\hat{R}_j^\top\xi = \hat{R}_j^\top\hat{R}_j\lambda$, which, in turn, yields

$$\hat{R}_j^\top\left(\xi - \hat{R}_j\lambda\right) = 0. \tag{26}$$

  Clearly, there is no unique solution to this equation. Consider a solution that satisfies $\xi - \hat{R}_j\lambda \neq 0$. Since the columns of $\hat{R}_j$ both belong to the plane defined by $\ker(\Pi)$, it must hold that the vector $\xi - \hat{R}_j\lambda$ is perpendicular to this plane. However, since $\hat{R}_j\lambda \in \ker(\Pi)$, this contradicts the assumption that $\xi \in \ker(\Pi)$. As such, the only solution that can satisfy (26) when $\Pi\xi = 0$ holds, is $\xi = \hat{R}_j\lambda$. For $\lambda \geq 0$ this implies $\xi \in \text{pos}\left\{r_1^j, r_2^j\right\} = \mathcal{T}_j$. □

Proposition 2. *Consider a simplicial partition $\mathcal{S}$ of $\mathcal{F}$. Define the set $\bar{\mathcal{R}}_\mathcal{S} := \mathcal{R}_\mathcal{S} \setminus \left\{[0, 0, -1]^\top\right\}$, and collect its elements in the matrix $\bar{R} := \left[r_1, \ldots, r_p\right] \in \mathbb{R}^{3\times p}$. Let the matrices $E_i \in \mathbb{R}^{p\times 3}$, $i \in \mathcal{N}$ have its qth row equal to zero for all $q \in \{1, \ldots, p\}$ such that $r_q \notin \mathcal{S}_i$, and the remaining rows equal to the rows of a three-dimensional identity matrix such that $\bar{R}E_i = R_i$. Here, no distinction is made between $r_q = [0, 0, 1]^\top$ and $r_q = [0, 0, -1]^\top$. Then the matrices*

$$F_i = E_i\left(\bar{R}E_i\right)^{-1}, \quad i \in \mathcal{N}, \tag{27}$$

satisfy the property $F_i\xi = F_j\xi$ for all $\xi \in \mathcal{S}_i \cap \mathcal{S}_j$ and $\xi \in -\mathcal{S}_i \cap -\mathcal{S}_j$, $i, j \in \mathcal{N} \times \mathcal{N}$, $i \neq j$, and all $\xi \in \mathcal{S}_i \cap -\mathcal{S}_j$, $i, j \in \mathcal{N} \times \mathcal{N}$.

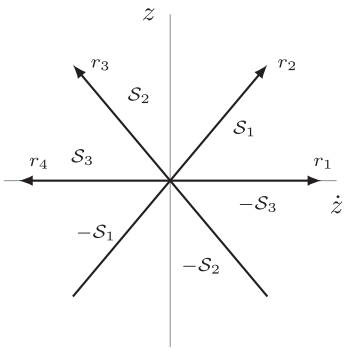

Fig. 6. Partitioning of the $(z, \dot{z})$-space.

Proof. The proof follows similar arguments as in [25, Section A.4]. First, the continuity property is shown for all $\xi \in \mathcal{S}_i \cap \mathcal{S}_j$, $i, j \in \mathcal{N} \times \mathcal{N}$, $i \neq j$. Observe that each $\xi \in \mathcal{S}_i$ can be written as a linear combination of elements from $\bar{\mathcal{R}}_{\mathcal{S}}$, such that

$$\xi = \sum_{q=1}^{p} r_q w_q = \bar{R} w^i, \tag{28}$$

where $w^i = [w_1^i, \ldots, w_p^i]^\top \in \mathbb{R}^p$ collects the weights. One can set $w_q^i = 0$ for all q such that $r_q \notin \mathcal{S}_i$ (where no distinction is made between $r_q = [0, 0, 1]^\top$ and $r_q = [0, 0, -1]^\top$). By doing so, it follows that $w^i = E_i E_i^\top w^i$, such that (28) can equivalently be written as $\xi = \bar{R} E_i E_i^\top w^i$. Since E_i extracts those columns from $\bar{R}$ that coincide with the generators of $\mathcal{S}_i$, it follows that the columns of the matrix $\bar{R}E_i$ are linearly independent and thus $\bar{R}E_i$ is invertible. From this, one finds the mapping $w_i = E_i \left(\bar{R}E_i\right)^{-1} \xi$. On the boundary shared by two simplicial cones $\mathcal{S}_i$ and $\mathcal{S}_j$, the only nonzero elements of w_i, w_j are those that describe this common boundary. Therefore, $w_i(\xi) = w_j(\xi)$ for all $\xi \in \mathcal{S}_i \cap \mathcal{S}_j$. The result trivially follows for $\xi \in -\mathcal{S}_i \cap -\mathcal{S}_j$, $i, j \in \mathcal{N} \times \mathcal{N}$, $i \neq j$.

It remains to show that (27) also yields the continuity property for $\xi \in \mathcal{S}_i \cap -\mathcal{S}_j$, $i, j \in \mathcal{N} \times \mathcal{N}$ which corresponds to the line $\xi = [0, 0, \dot{z}]^\top$. Since $[0, 0, -1]^\top$ is excluded, this common boundary is represented by only one column in $\bar{R}$, being $[0, 0, 1]^\top$. Therefore, for each $\xi \in \mathcal{S}_i \cap -\mathcal{S}_j$, $i, j \in \mathcal{N} \times \mathcal{N}$, the only nonzero element in w_i and w_j describes this common boundary. This concludes the proof. □

Example 1. In order to emphasize the subtlety in Proposition 2 of making no distinction between the vectors $[0, 0, \pm 1]^\top$ for constructing the continuity matrices, consider Fig. 6 which shows an example of a simplicial partitioning of the two-dimensional $(z, \dot{z})$-plane.

The generating set $\mathcal{R}_{\mathcal{S}}$ of the partitioning in Fig. 6 is given by $\mathcal{R}_{\mathcal{S}} = \{r_1, r_2, r_3, r_4\}$, with generators

$$r_1 = \begin{bmatrix} 1 \\ 0 \end{bmatrix}, r_2 = \begin{bmatrix} \frac{1}{2} \\ \frac{1}{2}\sqrt{3} \end{bmatrix}, r_3 = \begin{bmatrix} -\frac{1}{2} \\ \frac{1}{2}\sqrt{3} \end{bmatrix}, r_4 = \begin{bmatrix} -1 \\ 0 \end{bmatrix},$$

and $\bar{\mathcal{R}}_{\mathcal{S}} = \mathcal{R}_{\mathcal{S}} \setminus \{r_4\}$. The selection matrices are given by

$$E_1 = \begin{bmatrix} 1 & 0 \\ 0 & 1 \\ 0 & 0 \end{bmatrix}, E_2 = \begin{bmatrix} 0 & 0 \\ 1 & 0 \\ 0 & 1 \end{bmatrix}, \text{ and } E_3 = \begin{bmatrix} 1 & 0 \\ 0 & 0 \\ 0 & 1 \end{bmatrix},$$

and the continuity matrices follow as

$$F_1 = \begin{bmatrix} 1 & -\frac{1}{3}\sqrt{3} \\ 0 & \frac{2}{3}\sqrt{3} \\ 0 & 0 \end{bmatrix}, F_2 = \begin{bmatrix} 0 & 0 \\ 1 & \frac{1}{3}\sqrt{3} \\ -1 & \frac{1}{3}\sqrt{3} \end{bmatrix}, F_3 = \begin{bmatrix} 1 & \frac{1}{3}\sqrt{3} \\ 0 & 0 \\ 0 & \frac{2}{3}\sqrt{3} \end{bmatrix}.$$

Consider the point $\xi = (\dot{z}, z) = (\frac{1}{2}, \frac{1}{2}\sqrt{3})$ which is located on the boundary between the region $\mathcal{S}_1$ and $\mathcal{S}_2$. For this point one finds $F_1\xi = F_2\xi = [0, 1, 0]^\top$. Consider also the point $\xi = (\dot{z}, z) = (-1, 0)$, which is located on the boundary between $\mathcal{S}_3$ and $-\mathcal{S}_1$. In this case one has $F_1\xi = F_3\xi = [-1, 0, 0]^\top$. If the vector r_4 would have been taken into account for constructing the matrices F_i, $i = 1, 2, 3$, then one finds for $\xi = (-1, 0)$ that $F_1\xi = [-1, 0, 0, 0]^\top$ and $F_3\xi = [0, 0, 0, 1]^\top$. In that case the continuity property does not hold over the boundary shared by the regions $\pm\mathcal{S}_1$ and $\mp\mathcal{S}_3$ as this boundary is described by two different vectors in $\bar{\mathcal{R}}_{\mathcal{S}}$. Elimination of the vector r_4 (alternatively r_1) ensures that this boundary is represented by a single vector in $\bar{\mathcal{R}}_{\mathcal{S}}$.

In order to use the matrices S_i, T_j and F_i for an LMI based analysis of the closed-loop system in (12), these are transformed to

$$\bar{S}_i = S_i H, \quad \bar{T}_j = T_j H, \quad \text{and } \bar{F}_i = \begin{bmatrix} (F_i H)^\top, I \end{bmatrix}^\top, \tag{29}$$

where H is defined in (13), and the continuity matrix is appended with an identity matrix for ensuring full rank.

It is important to stress that the simplicial partitioning presented in this paper does not introduce any conservatism in the analysis as compared to the approach in [21]. Since each polyhedral cone with non-empty interior can be partitioned into a finite number of simplicial cones [30, Lemma 1.40], when defining a continuous function over a polyhedral partitioning such as discussed in [21], this same function can be defined over a simplicial partitioning as well. The converse, however, is not necessarily true, thereby indicating improved flexibility of the simplicial partitioning proposed here.

Remark 1. If the input signals w are directly input to the HIGS, z and $\dot{z}$ depend on x, w, and $\dot{w}$. Consequently, due to the specific partitioning of $\mathcal{F}$ and the construction of the continuity matrices F_i as in Proposition 2, a function of the form (15) becomes dependent on w and $\dot{w}$. Different from the approach in [14] in which dependency of the partitioning on the inputs necessarily led to a common quadratic function rather than a piecewise quadratic one (see also the discussion in [14, Section 4.2]), here this dependency is not necessarily restrictive. However, it requires knowledge about w and $\dot{w}$, which may generally not be available. In the current setting this is dealt with by Assumption 1. In case specific knowledge is available, input (impulse response) filters can be used to embed this knowledge in (15) as reflected by the filter state variables corresponding to w and $\dot{w}$. In that case, one may also relax the assumption on the relative degree of the transfer function $\Sigma_{zw}(s)$ in (11).

4.2. Main results

Before presenting the main results, appropriate definitions for input-to-state stability and $\mathcal{L}_2$-gain are given.

Definition 5. The HIGS-controlled system (12) is said to be pre-input-to-state stable (pre-ISS), if there exist a $\mathcal{KL}$-function σ and a $\mathcal{K}$-function ϕ such that for any initial condition $x(0) = x_0 \in \mathbb{R}^{p+1}$ and any bounded input signal w, all corresponding solutions to (12) satisfy

$$\|x(t)\| \leq \sigma\left(\|x(0)\|, t\right) + \phi\left(\sup_{0\leq\tau\leq t} \|w(\tau)\|\right), \tag{30}$$

for all $t \in \operatorname{dom} x$.

Definition 6. The $\mathcal{L}_2$-gain of the HIGS-controlled system (12) subject to input w is defined as

$$\|\Sigma\|_\infty = \sup_{\substack{w\in\mathcal{L}_2\setminus\{0\} \\ \operatorname{dom} q_w \neq \{0\}}} \frac{\|q_w\|_2}{\|w\|_2}, \tag{31}$$

where q_w is the output satisfying (12) with $x(0) = 0$, and $\|\cdot\|_2$ denotes the $\mathcal{L}_2$-norm, which is defined as $\|v\|_2 = (\int_0^{T_v} \|v(t)\|^2 dt)^{1/2}$ with $T_v = \sup \operatorname{dom} v$.

Remark 2. The notion of pre-ISS and $\mathcal{L}_2$-gain on possibly finite time intervals is adopted to indicate the possibility of (maximal) solutions not being forward complete, *e.g.,* solutions of which the domain is not defined for all times $t \in \mathbb{R}_{\geq 0}$. Allowing for this situation separates conditions for forward completeness of solutions from conditions on stability and performance, see also the discussion in [37, Section 3.1] and [15, Remark 5]. For inputs to (12) that belong to the class of piecewise Bohl functions, see [21, Definition 2], forward completeness of solutions (*i.e.,* $\sup \operatorname{dom} x = \infty$) can be formally guaranteed [21,33].

Theorem 1. *Consider the system given in (12) with $w \in \mathcal{L}_2$, and let $\mathcal{S}$ be a simplicial partition of $\mathcal{F}$. Suppose there exist matrices $U_i, W_i \in \mathbb{S}^{3\times 3}_{\geq 0}$ for all $i \in \mathcal{N}$, and $V_i \in \mathbb{S}^{2\times 2}_{\geq 0}$, $L_i \in \mathbb{R}^q$ for all $i \in \mathcal{M}$, a matrix $\Phi \in \mathbb{S}^{q\times q}$, and constant $\gamma > 0$, such that $P_i = \bar{F}_i^\top \Phi \bar{F}_i$ satisfies the following LMI conditions:*

$$P_i - \bar{S}_i^\top W_i \bar{S}_i \succ 0, \quad \text{for all } i \in \mathcal{N}, \tag{32}$$

$$\begin{bmatrix} \hat{A}_k^\top P_i + P_i \hat{A}_k + G_{i,k} & P_i B_k & C^\top \\ B_k^\top P_i & -\gamma I & D^\top \\ C & D & -\gamma I \end{bmatrix} \prec 0, \tag{33}$$

for $(k, i) \in (\{1\} \times \mathcal{N}) \cup (\{2\} \times \mathcal{M})$), in which $\hat{A}_1 = A_1$, and $\hat{A}_2 = A_2 + \Delta$, with

$$\Delta = \alpha \begin{bmatrix} 0 & \Lambda^\top \end{bmatrix}^\top, \tag{34}$$

with $\alpha \in \mathbb{R}$ a fixed number, $\Lambda = \Pi H$, and

$$G_{i,1} = \bar{S}_i^\top U_i \bar{S}_i, \tag{35a}$$

$$G_{i,2} = \bar{T}_i^\top V_i \bar{T}_i + L_i \Lambda + (L_i \Lambda)^\top, \tag{35b}$$

where $\bar{S}_i$, $\bar{T}_i$, and $\bar{F}_i$ are given in (29). Then for all $x(0) \in \mathbb{R}^{p+1}$, the closed-loop system in (12) is pre-ISS and has a finite $\mathcal{L}_2$-gain from w to q smaller than or equal to γ.

Remark 3. The motivation for using the extended system matrix $\hat{A}_2 = A_2 + \Delta$ rather than A_2, comes from numerical considerations. Since A_2 results from explicit differentiation of the algebraic constraint in gain-mode, this matrix is singular. Consequently, the LMI problem in (32), (33) becomes ill-conditioned, which potentially leads to numerical issues; note that this corresponds to $\alpha = 0$ in (34). By appending A_2 with an additional matrix Δ, the resulting matrix $\hat{A}_2$ becomes non-singular, thereby leading to numerically more favourable conditions. Note that the gain-mode dynamics remain unchanged, that is, $A_2 x = \hat{A}_2 x$ for all $Hx \in \mathcal{F}_2$. A suitable choice for α may be one that minimizes the condition number of $\hat{A}_2$.

Proof. Consider the piecewise quadratic function

$$V(x) = V_i(x) := x^\top P_i x, \text{ when } Hx \in \mathcal{S}_i,\ i \in \mathcal{N}, \tag{36}$$

with $P_i = \bar{F}_i^\top \Phi \bar{F}_i$. The proof is based on showing that under the conditions of the theorem, (36) classifies as a suitable storage function with supply rate matching $\mathcal{L}_2$-gain guarantees [38,39] for the closed-loop system (12), and simultaneously qualifies as a non-smooth ISS Lyapunov function, see, *e.g.*, [35, Definition 3.2].

First, observe that V is composed by locally Lipschitz continuous functions. By virtue of Proposition 2, V is continuous over the boundaries of the partitioning, making V a (non-smooth) locally Lipschitz continuous function on $\{x \in \mathbb{R}^n \mid Hx \in \mathcal{F}\}$.

Positive definiteness of V is implied by (32). Indeed, from the results in Proposition 1 and non-negativity of the elements in W_i, it follows that

$$x^\top \bar{S}_i^\top W_i \bar{S}_i x \geq 0, \text{ when } x \in \mathcal{S}_i,\ i \in \mathcal{N}. \tag{37}$$

Application of the S-procedure then shows that

$$V(x) > x^\top \bar{S}_i^\top W_i \bar{S}_i x \geq 0 \text{ if } 0 \neq x \in \mathcal{S}_i,\ i \in \mathcal{N}. \tag{38}$$

The strict inequality implies the existence of some sufficiently small $\alpha_1 > 0$ such that $V(x) \geq \alpha_1 \|x\|^2$. Furthermore, due to the piecewise quadratic construction of V there exists $\alpha_2 > 0$ such that $V(x) \leq \alpha_2 \|x\|^2$. Hence, one finds

$$\alpha_1 \|x\|^2 \leq V(x) \leq \alpha_2 \|x\|^2, \tag{39}$$

which yields the corresponding result.

Since solutions to (12) are locally absolutely continuous, the composite function $t \mapsto V(x(t))$ is locally absolutely continuous and almost everywhere differentiable with respect to time, *i.e.*, $\frac{d}{dt} V(x(t))$ exists almost everywhere.

Next, it is shown that for $(k, i) \in \{1\} \times \mathcal{N} \cup \{2\} \times \mathcal{M}$ condition (33) implies

$$\frac{d}{dt} V(x(t)) \leq -\epsilon \|x(t)\|^2 - \|q(t)\|^2 + \gamma^2 \|w(t)\|^2 \tag{40}$$

to hold almost everywhere. Following the same arguments as in [35, Theorem 3.3], it can be concluded that for almost all times t

$$\frac{d}{dt} V(x(t)) \leq \max_{(k,i) \in \mathcal{KI}} \nabla V_i(x(t)) \left(A_k x(t) + B w(t)\right), \tag{41}$$

where $\mathcal{KI} := \{1\} \times \mathcal{N} \cup \{2\} \times \mathcal{M}$. In integrator-mode, $\nabla V_i(x)(A_1 x + Bw)$ evaluates to

$$\nabla V_i(x)(A_1 x + Bw) = x^\top \left(A_1^\top P_i + P_i A_1\right) x + 2 x^\top P_i B w,$$

for all $i \in \mathcal{N}$. Using the results from Proposition 1, and non-negativity of the elements in U_i, one finds that $x^\top G_{i,1} x \geq 0$ when $Hx \in \mathcal{S}_i$. Application of the S-procedure in combination with the Schur complement of (33) shows that the inequality in (33) implies for $k = 1$, $i \in \mathcal{N}$ that

$$\begin{aligned}
&\nabla V_i(x)(A_1 x + Bw) = x^\top \left(A_1^\top P_i + P_i A_1\right) x + 2 x^\top P_i B w \\
&\leq -\epsilon \|x\|^2 - (Cx + Dw)^\top (Cx + Dw) + \gamma^2 \|w\|^2 \\
&= -\epsilon \|x\|^2 - \|q\|^2 + \gamma^2 \|w\|^2.
\end{aligned}$$

In a similar manner, in gain-mode one finds

$$\nabla V_i(x)(A_2 x + Bw) = x^\top \left(A_2^\top P_i + P_i A_2\right) x + 2 x^\top P_i B w,$$

for all $i \in \mathcal{M}$. Combining the results of Proposition 1 with non-negativity of the elements in V_i shows that $x^\top G_{i,2} x \geq 0$ for all $Hx \in \mathcal{T}_i$. Application of the S-procedure, Finsler's lemma and the Schur complement then shows that the inequality in (33) for $k = 2$, $i \in \mathcal{M}$ implies

$$\begin{aligned}\nabla V_i(x)(A_2x + Bw) &= x^\top \left(A_2^\top P_i + P_i A_2\right) x + 2x^\top P_i B w + \underbrace{2x^\top P_i \Delta x}_{=0} \\ &\leq -\epsilon \|x\|^2 - (Cx + Dw)^\top (Cx + Dw) + \gamma^2 \|w\|^2 \\ &= -\epsilon \|x\|^2 - \|q\|^2 + \gamma^2 \|w\|^2,\end{aligned}$$

where the algebraic relation $\Delta x = 0$ is used, which holds true for all $Hx \in \mathcal{T}_i$, $i \in \mathcal{M}$. From this, one may conclude that the upper-bound on the time-derivative of V as in (40) holds almost everywhere. The proof can be completed in a standard manner by using well-known comparison results, see, *e.g.*, [40]. □

Besides the $\mathcal{L}_2$-gain, which is typically considered as a steady-state root-mean-square (RMS) gain, one is often interested in measures reflecting the transient performance of a system. For linear systems, such a measure is given by the $\mathcal{H}_2$-norm, which, amongst others, can be interpreted as the energy in the response of the system to an impulse (starting from an initial condition $x(0) = 0$) [41]. This characterization has been extended to reset control systems in [14]. In the following, the approach presented in [14] is adopted for calculating the $\mathcal{H}_2$-norm for HIGS-controlled systems. In particular, through the use of stable input filters, the energy in the response of the system subject to specific input signals, such as a step input or a sinusoid, can be approximated. Note that for the system in (12) the impulse response is obtained by setting $w(t) = 0$ for all $t \in \mathbb{R}_{\geq 0}$, and considering an appropriate set of non-zero initial conditions $x(0) = B$ that correspond to unitary impulses on the input channels. Conform Remark 2, since $w = 0$ is a "Bohl input", forward completeness of solutions is guaranteed. The $\mathcal{H}_2$-norm is defined as follows.

Definition 7. The $\mathcal{H}_2$-norm of a HIGS-controlled system (12) corresponding to an initial value $x(0) = x_0 = B$ is defined as

$$\|\Sigma\|_{2,x_0} = \|q\|_{2,T}, \tag{42}$$

where q is the output satisfying (12) with $w = 0$, $x(0) = B$ and $T = \sup \operatorname{dom} q$.

Theorem 2. *Consider the system in (12) with $w = 0$ and initial condition $x(0) = x_0 = B$. Let $\mathcal{S}$ be a simplicial partitioning of $\mathcal{F}$. Suppose there exist matrices U_i, $W_i \in \mathbb{S}^{3\times 3}_{\geq 0}$, $V_i \in \mathbb{S}^{2\times 2}_{\geq 0}$, $L_i \in \mathbb{R}^q$, $\Phi \in \mathbb{S}^{q\times q}$, and a constant $\gamma > 0$, such that $P_i = \bar{F}_i^\top \Phi \bar{F}_i$ satisfies:*

$$P_i - \bar{S}_i^\top W_i \bar{S}_i \succ 0, \tag{43}$$

$$\hat{A}_k^\top P_i + P_i \hat{A}_k + G_{i,k} + C^\top C \prec 0, \tag{44}$$

$$\gamma^2 - B^\top P_j B \geq 0, \tag{45}$$

for $(k, i) \in (\{1\} \times \mathcal{N}) \cup (\{2\} \times \mathcal{M}))$, with $\hat{A}_1 = A_1$, $\hat{A}_2 = A_2 + \Delta$, $G_{i,k}$ defined in (35), and $j \in \mathcal{J}(x_0) := \{i \in \mathcal{N} \mid x_0 \in \mathcal{S}_i\}$. Then, the closed-loop system (12) is exponentially stable with $\mathcal{H}_2$-norm for initial condition x_0 smaller than or equal to γ.

Proof. Similar to the proof of Theorem 1, now with $w = 0$, conditions (43), (44) imply $\|\Sigma\|^2_{2,x_0} = \|q\|_2^2 \leq V(x_0)$. Using (45) with $x_0 = B$ one finds

$$\|q\|_2 \leq \gamma, \tag{46}$$

which yields an upper-bound on $\|\Sigma\|_{2,x_0}$ defined in (42). Exponential stability immediately follows from the proof of Theorem 1 with $w = 0$. This completes the proof. □

Remark 4. It is well-known [37] that robust stability issues can arise in a discontinuous piecewise-linear system such as (12). For obtaining robust stability guarantees, one may consider the Krasovskii regularization of a discontinuous dynamical system. Similar to [21], the Krasovskii regularization of (12) is formulated as

$$\dot{x} \in \begin{cases} A_1 x + B_1 w & \text{if } Hx \in \mathcal{F}_1 \setminus \overline{\mathcal{F}}_2, \\ \operatorname{co}(A_1 x + B_1 w, A_2 x + B_2 w) & \text{if } Hx \in \overline{\mathcal{F}}_2, \end{cases} \tag{47}$$

in which $\operatorname{co}(\mathcal{X})$ denotes the closed convex hull of a set $\mathcal{X} \subset \mathbb{R}^n$. Different from the original system description in (12) which does not possess sliding-modes, the Krasovskii regularized system in (47) allows convex combinations of the integrator- and gain-mode dynamics at certain states. In this regard, note that within a cell $\mathcal{S}_i \subset \overline{\mathcal{F}}_1$ of the partitioning that contains a boundary plane $\mathcal{T}_j \subset \overline{\mathcal{F}}_2$ (see also Fig. 5), a "common quadratic function" $V(x) = x^\top P_i x$ is defined so that on this boundary plane the LMI conditions in Theorems 1 and 2 hold true for the convex combination of integrator- and gain-mode dynamics, and thus for the Krasovskii regularized dynamics in (47). As such, Theorems 1 and 2 provide certain robust stability and performance guarantees, see also [21, Remark 8].

Remark 5. Regarding the computational complexity of the LMIs in Theorems 1 and 2, note that the number of decision variables $\mathcal{D}$ in the LMIs scales at least proportionally to the number of partitionings according to $\mathcal{D} \propto 2N + M$. Depending on the solver, the numerical complexity of the LMI conditions may, in turn, scale proportionally to $\mathcal{D}^3$, see, for instance [42]. Though mathematically there is no a priori limit on the maximum number of partitions, the increasing computational burden may pose a practical limit.

4.3. On infeasibility of the LMI conditions

When the LMIs in Theorem 1 or Theorem 2 turn out to be infeasible for a certain partitioning, this partitioning can be iteratively refined to increase the possibility of finding a solution, if existing. In this regard, it might be useful to know in advance under which conditions and for which partitioning the LMIs will not be feasible, such that these cases do not have to be considered. In general, this is difficult to assess since the LMI conditions are only sufficient. However, some insights can be obtained into infeasibility of the LMIs when one or both submodes of the HIGS-controlled system are unstable. This is formalized in the following proposition.

Proposition 3. *Let a simplicial partitioning $\mathcal{S}$ of $\mathcal{F}$ be given. The LMI conditions in Theorems 1 and 2 do not admit a feasible solution for that specific $\mathcal{S}$ if one (or both) of the following conditions holds.*

C1. *The matrix A_1 given in (14) has eigenvalues $\lambda \in \mathbb{C}$ with $\mathrm{Re}(\lambda) > 0$ that satisfy for some $i \in \mathcal{N}$*

$$\left\{ \begin{bmatrix} \mathrm{Re}(\lambda) \\ \omega_h \\ \mathrm{Re}(\lambda)^2 - \mathrm{Im}(\lambda)^2 \end{bmatrix}, \begin{bmatrix} \mathrm{Im}(\lambda) \\ 0 \\ 2\mathrm{Re}(\lambda)\mathrm{Im}(\lambda) \end{bmatrix} \right\} \subset \mathcal{S}_i \cup -\mathcal{S}_i. \tag{48}$$

C2. *The matrix $A_l + k_h B_u C_z$ with A_l, B_u, C_z given in (7) has eigenvalues $\lambda \in \mathbb{C}$ with $\mathrm{Re}(\lambda) > 0$ that satisfy for some $i \in \mathcal{M}$*

$$\left\{ \begin{bmatrix} 1 \\ \mathrm{Re}(\lambda) \end{bmatrix}, \begin{bmatrix} 0 \\ \mathrm{Im}(\lambda) \end{bmatrix} \right\} \subset \mathcal{T}_i \cup -\mathcal{T}_i. \tag{49}$$

Proof. For proving infeasibility of the LMIs (32), (33) and (43)–(45), it is sufficient to prove that the LMIs

$$P_i - \bar{S}_i^\top W_i \bar{S}_i \succ 0, \tag{50a}$$

$$\hat{A}_k^\top P_i + P_i \hat{A}_k + G_{i,k} \prec 0, \tag{50b}$$

with $G_{i,k}$ defined in (35) and $\bar{S}_i$ given in (29), cannot be feasible for some $(k, i) \in \{1\} \times \mathcal{N} \cup \{2\} \times \mathcal{M}$ under conditions (48) and/or (49).

C1. Consider the integrator-mode subsystem ($k = 1$). If feasible, the conditions in (50) imply that for any complex nonzero vector $v \in \mathbb{C}^m$ and its complex conjugate $\bar{v}$ the inequalities

$$\bar{v}^\top \left(P_i - \bar{S}_i^\top W_i \bar{S}_i \right) v > 0 \quad \text{and} \quad \bar{v}^\top \left(A_1^\top P_i + P_i A_1 + \bar{S}_i^\top U_i \bar{S}_i \right) v < 0$$

are satisfied. Choose v to be an eigenvector of A_1 such that $A_1 v = \lambda v$ with $\lambda \in \mathbb{C}$ the corresponding eigenvalue. Observe the identity

$$Hv \overset{(13)}{=} \begin{bmatrix} C_z & 0 \\ 0 & 1 \\ C_z A_l & 0 \end{bmatrix} v = \begin{bmatrix} \frac{1}{\omega_h} C_u A_1 \\ C_u \\ \frac{1}{\omega_h} C_u A_1^2 \end{bmatrix} v = \rho C_u v \tag{51}$$

with $C_u := [0_{1\times p}, 1]$, $\rho := \begin{bmatrix} \frac{\lambda}{\omega_h} & 1 & \frac{\lambda^2}{\omega_h} \end{bmatrix}^\top$ and the matrices C_z, A_1 are given in (7) and (14), respectively. Note that here use is made of the fact that $C_z B_u = 0$. Assume $\lambda \in \mathbb{C}$ such that

$$\rho = \frac{1}{\omega_h} \left(\begin{bmatrix} \mathrm{Re}(\lambda) \\ \omega_h \\ \mathrm{Re}(\lambda)^2 - \mathrm{Im}(\lambda)^2 \end{bmatrix} + j \begin{bmatrix} \mathrm{Im}(\lambda) \\ 0 \\ 2\mathrm{Re}(\lambda)\mathrm{Im}(\lambda) \end{bmatrix} \right). \tag{52}$$

By construction of $\bar{S}_i$ as in (29), it follows that

$$\begin{aligned} \bar{S}_i v &= R_i^{-1} H v = R_i^{-1} \rho C_u v \\ &= R_i^{-1} \left(\mathrm{Re}(\rho) + j\mathrm{Im}(\rho) \right) C_u v. \end{aligned} \tag{53}$$

Note that additionally

$$\bar{S}_i \bar{v} = R_i^{-1} \left(\mathrm{Re}(\rho) - j\mathrm{Im}(\rho) \right) C_u \bar{v}.$$

If $\mathrm{Re}(\rho), \mathrm{Im}(\rho) \in \mathcal{S}_i$ then $R_i^{-1}\mathrm{Re}(\rho) \geq 0$ and $R_i^{-1}\mathrm{Im}(\rho) \geq 0$ hold entry-wise. Similarly, for $\mathrm{Re}(\rho), \mathrm{Im}(\rho) \in -\mathcal{S}_i$ one has $R_i^{-1}\mathrm{Re}(\rho) \leq 0$ and $R_i^{-1}\mathrm{Im}(\rho) \leq 0$. Moreover, if $\mathrm{Re}(\rho) \in \pm\mathcal{S}_i$ and $\mathrm{Im}(\rho) \in \mp\mathcal{S}_i$, then $R_i^{-1}\mathrm{Re}(\rho)$ and $R_i^{-1}\mathrm{Im}(\rho)$ have opposite signs. For any symmetric matrix X_i with non-negative elements one finds

$$\bar{v}^\top S_i^\top X_i S_i v = \bar{v}^\top C_u^\top \begin{bmatrix} \mathrm{Re}(\rho) \\ \mathrm{Im}(\rho) \end{bmatrix}^\top Q_i \begin{bmatrix} \mathrm{Re}(\rho) \\ \mathrm{Im}(\rho) \end{bmatrix} C_u v \geq 0, \tag{54}$$

with $Q_i = \mathrm{diag}\left(R_i^{-\top} X_i R_i^{-1}, R_i^{-\top} X_i R_i^{-1}\right)$ a block diagonal matrix. Note that the cross product of real and imaginary parts cancels. Suppose (50a) holds. Through (54) with $X_i = W_i$, this implies $\bar{v}^\top P_i v > 0$, which, in turn, for $\mathrm{Re}(\lambda) > 0$ implies

$$\begin{aligned} &\bar{v}^\top \left(A_1^\top P_i + P_i A_1\right) v + \bar{v}^\top \bar{S}_i^\top U_i \bar{S}_i v \\ &= 2\mathrm{Re}(\lambda)\bar{v}^\top P_i v + \bar{v}^\top \bar{S}_i^\top U_i \bar{S}_i v > 0. \end{aligned} \tag{55}$$

Hence, under condition (48) the inequalities in (50) cannot be satisfied, which shows that the LMIs in Theorems 1 and 2 are infeasible in this case.

C2. Consider the gain-mode subsystem ($k = 2$). As these dynamics are defined in a lower-dimensional region of $\mathcal{F}$, namely $\mathcal{F}_2$ in (5b), it follows from Finsler's lemma that for $k = 2$ and any $i \in \mathcal{M}$, the LMIs in (50) can equivalently be written as

$$\Theta^\top \left(P_i - \bar{S}_i^\top W_i \bar{S}_i\right) \Theta \succ 0, \tag{56a}$$

$$\Theta^\top \left(A_2^\top P_i + P_i A_2\right) \Theta + \Theta^\top \bar{T}_i^\top V_i \bar{T}_i \Theta \prec 0, \tag{56b}$$

with $\Theta = [I, k_h C_z^\top]^\top$ and A_2 is given in (14). Next, observe that

$$A_2\Theta = \begin{bmatrix} A_l & B_u \\ k_h C_z A_l & 0 \end{bmatrix} \begin{bmatrix} I \\ k_h C_z \end{bmatrix} = \begin{bmatrix} A_l + k_h B_u C_z \\ k_h C_z A_l \end{bmatrix} = \Theta \bar{A}_2,$$

where $\bar{A}_2 := A_l + k_h B_u C_z$ with A_l, B_u, C_z given in (14), and use is made of the fact that $C_z B_u = 0$. Consider $v \in \mathbb{C}^{m-1}$ to be an eigenvector of $\bar{A}_2$ such that $\bar{A}_2 v = \lambda v$ with $\lambda \in \mathbb{C}$ the corresponding eigenvalue. Then the following identity holds

$$H\Theta v = \begin{bmatrix} C_z & 0 \\ 0 & 1 \\ C_z A_l & 0 \end{bmatrix} \begin{bmatrix} I \\ k_h C_z \end{bmatrix} v = \begin{bmatrix} C_z \\ k_h C_z \\ C_z \bar{A}_2 \end{bmatrix} v = \rho C_z v, \tag{57}$$

with $\rho := \begin{bmatrix} 1 & k_h & \lambda \end{bmatrix}^\top$. Assume $\lambda \in \mathbb{C}$ such that

$$\rho = \begin{bmatrix} 1 \\ k_h \\ \mathrm{Re}(\lambda) \end{bmatrix} + j \begin{bmatrix} 0 \\ 0 \\ \mathrm{Im}(\lambda) \end{bmatrix}. \tag{58}$$

The vectors $\mathrm{Re}(\rho)$ and $\mathrm{Im}(\rho)$ both belong to the plane in $\mathcal{F}$ defined by $\Pi\xi = [k_h, -1, 0]\xi = 0$, $\xi \in \mathbb{R}^3$, *i.e.,* the two-dimensional plane in $\mathcal{F}$ on which the gain-mode is defined. Consequently, since $\mathcal{T}_i$, $i \in \mathcal{M}$ is a subset of this plane, and $\mathcal{T}_i \subset \mathcal{S}_i$ for all $i \in \mathcal{M}$, it follows that

$$\left\{ \begin{bmatrix} 1 \\ \mathrm{Re}(\lambda) \end{bmatrix}, \begin{bmatrix} 0 \\ \mathrm{Im}(\lambda) \end{bmatrix} \right\} \subset \mathcal{T}_i \Leftrightarrow \{\mathrm{Re}(\rho), \mathrm{Im}(\rho)\} \subset \mathcal{S}_i.$$

Using a similar reasoning as before, it follows that if (49) is true, then the inequalities $\bar{v}^\top \Theta \bar{S}_i^\top W_i \bar{S}_i \Theta v \geq 0$ and $\bar{v}^\top \Theta \bar{T}_i^\top V_i \bar{T}_i \Theta v \geq 0$ hold. Suppose (56a) is feasible. Together with the above this implies $\bar{v}^\top \bar{P}_i v > 0$ with $\bar{P}_i := \Theta^\top P_i \Theta$. Consequently it must be true that

$$\begin{aligned} &\bar{v}^\top \left(\bar{A}_2^\top \bar{P}_i + \bar{P}_i \bar{A}_2\right) v + v^* \Theta \bar{T}_i^\top V_i \bar{T}_i \Theta v \\ &= 2\mathrm{Re}(\lambda)\bar{v}^\top \bar{P}_i v + \bar{v}^\top \Theta \bar{T}_i^\top V_i \bar{T}_i \Theta v > 0. \end{aligned} \tag{59}$$

This contradicts (56), which implies that (50) cannot be feasible when (49) is true. In turn, this shows that for this case the LMIs in Theorems 1 and 2 cannot be feasible. This completes the proof. □

The result of Proposition 3 clearly shows the benefits of considering a partitioning in the full $(z, u, \dot{z})$-space in contrast to *e.g.,* a partitioning in the (z, u)-space as considered in [27]. Namely, when (48) and/or (49) are true, one can refine the partitioning to render these conditions false, whereas for a simpler partitioning such flexibility may be limited. For example, in case the gain-mode region is not partitioned, (49) is always satisfied for any eigenvalue λ of the matrix $A_l + k_h B_u C_z$ that satisfies $0 \leq \mathrm{Re}(\lambda) \leq \frac{\omega_h}{k_h}$ and $\mathrm{Im}(\lambda) \in \mathbb{R}$. When the gain-mode region is partitioned, this is not necessarily true. With these conditions one may test upfront if a simpler, computationally less demanding partitioning (recall Remark 5) could potentially work, or a more involved three-dimensional partitioning should be considered. The application and relevance of Proposition 3 is illustrated in Section 5.

Closer inspection of the results in Proposition 3 reveals that, under some simple conditions on the eigenvalues related to the system matrices in integrator-mode and gain-mode, there exists no partitioning for which the LMIs are feasible. These conditions are summarized in the following corollary.

Corollary 1. *The LMI conditions in Theorems 1 and 2 do not admit a feasible solution for any simplicial partitioning $\mathcal{S}$ of $\mathcal{F}$ if one or both of the following conditions hold:*

(i) there is a real eigenvalue λ of A_1 that satisfies $\lambda > \frac{\omega_h}{k_h}$;

(ii) there is a real eigenvalue λ of $A_l + k_h B_u C_z$ that satisfies $0 \leq \lambda < \frac{\omega_h}{k_h}$.

Proof. Consider the vectors

$$v_1 = \begin{bmatrix} \mathrm{Re}(\lambda) \\ \omega_h \\ \mathrm{Re}(\lambda)^2 - \mathrm{Im}(\lambda)^2 \end{bmatrix}, \quad \text{and} \quad v_2 = \begin{bmatrix} 1 \\ k_h \\ \mathrm{Re}(\lambda) \end{bmatrix}. \tag{60}$$

Suppose that (i) holds. Since $\mathrm{Im}(\lambda) = 0$ by assumption, it follows that $v_1 \in \mathcal{F}_1$. As $\mathcal{S}_i \subset \mathcal{F}_1$ for all $i \in \mathcal{N}$, there always exists a region $\mathcal{S}_i$ such that $v_1 \in \mathcal{S}_i$. Similarly, assume that (ii) holds such that $v_2 \in \mathcal{F}_2$. Since $\mathrm{Im}(\lambda) = 0$ and $\mathcal{T}_i \subset \mathcal{F}_1$ for all $i \in \mathcal{M}$, there always exists a region $\mathcal{T}_i$ such that $v_2 \in \mathcal{T}_i$. Consequently, condition (48) and/or (49) are satisfied for any partitioning, and thus the LMIs are not feasible. □

Interestingly, these algebraic conditions can directly be interpreted in terms of unstable closed-loop system behaviour. Indeed, the vectors v_1 and v_2 in (60) define a possible direction along which the $(z, u, \dot{z})$-trajectory can evolve in the sectors $\mathcal{F}_1$ or $\mathcal{F}_2$. When condition (i) in Corollary 1 is satisfied, the z-trajectory evolves at a rate of at least $1/k_h$ times faster than the u-trajectory, *i.e.,* $0 \leq du/dz < k_h$. Consequently, the sector boundary $u = k_h z$ cannot be reached such that potentially stabilizing switching is not initiated. A similar interpretation is given for the gain-mode. When condition (ii) is satisfied, the $\dot{z}$-trajectory evolves at least ω_h/k_h times slower than the z-trajectory. As such, $0 \leq d\dot{z}/dz < \omega_h/k_h$ and the switching boundaries $\omega_h z = k_h \dot{z}$ or $z = 0$ cannot be reached. Note that a condition on the magnitude of the eigenvalues is thus a consequence of the sector-boundedness of the HIGS. The above observations can even be translated into *necessary* conditions for input-to-state stability as formalized in the following theorem.

Theorem 3. *A necessary condition for the HIGS-controlled system (12) to be input-to-state stable (ISS) in the sense of Definition 6 is that none of the conditions in Corollary 1 hold.*

Proof. If the conditions in Corollary 1 are satisfied, then one (or both) of the sub-modes is unstable, and according to Corollary 1 it follows that the eigenvector $v \in \mathbb{R}^m$ corresponding to the unstable real eigenvalue satisfies $Hv \in \mathcal{F}_1$ or $H\Theta v \in \mathcal{F}_2$. When starting in the integrator-mode with initial condition $x(0) = v$ and $w = 0$, trajectories evolve according to $x(t) = e^{\lambda t} v$. For the integrator-mode one finds for all $t \geq 0$

$$(z(t), u(t), \dot{z}(t)) = e^{\lambda t} Hv \in \mathcal{F}_1. \tag{61}$$

Similarly, starting with initial condition $x(0) = \Theta v$ in gain-mode yields $x(t) = e^{\lambda t}\Theta v$ such that for $t \geq 0$

$$(z(t), u(t), \dot{z}(t)) = e^{\lambda t} H\Theta v \in \mathcal{F}_2. \tag{62}$$

The $(z, u, \dot{z})$-trajectory moves along the line spanned by $Hv \in \mathcal{F}_1$ or $H\Theta v \in \mathcal{F}_2$. The system cannot switch: it remains in the unstable linear mode and thus trajectories diverge exponentially from the origin. This directly violates the property of an ISS system that for zero inputs, the origin is asymptotically stable for any admissible initial condition $x_0 \in \mathbb{R}^{p+1}$ as implied by the upper-bound in (30). □

Remark 6. For planar HIGS-controlled systems, being the interconnection of HIGS with a one-dimensional plant, the conditions in Theorem 3 are necessary and sufficient, see also related results for reset systems in [43, Theorem 3] and linear complementary systems in [44, Theorem III.3].

Remark 7. The above results shed some light on the choices for ω_h and k_h in terms of feasibility of the LMIs, and thus provide initial direction toward parameter tuning. Namely, the algebraic conditions in Proposition 3 and Corollary 1 allow for finding a (possibly conservative) range for ω_h and k_h for which the LMIs will never admit a feasible solution (despite the partitioning), and as a result of Theorem 3 will lead to an unstable closed-loop system.

5. Numerical case study

In this section, applicability of the presented stability and performance analysis tools is demonstrated for the class of HIGS-controlled motion systems through simulated experiments. Particularly, the conservatism in the time-domain analysis is evaluated.

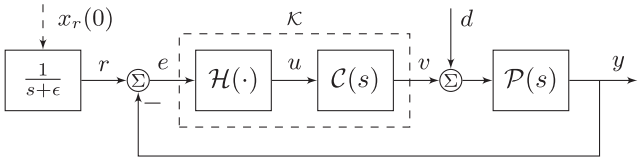

Fig. 7. Schematic representation of the closed-loop system considered in the numerical example.

5.1. System description and controller design

Consider a motion system represented by the fourth-order transfer function

$$\mathcal{P}(s) = \frac{1}{ms^2} - \frac{1}{m(s^2 + 2\beta_0\omega_0 s + \omega_0^2)}, \tag{63}$$

which is a combination of rigid-body and non-rigid-body dynamics, and where $m = 18$ kg, $\omega_0 = 1200 \cdot 2\pi$ rad/s, and $\beta_0 = 0.03$. This system is placed in feedback with a controller $\mathcal{K}$ being the series interconnection of a linear PID-filter $\mathcal{C}_{pid}(s)$, a second order low-pass filter $\mathcal{C}_{lp}(s)$, and a notch filter $\mathcal{C}_n(s)$. The individual filters are constructed as

$$\mathcal{C}_{pid}(s) = k_p\left(1 + \frac{\omega_i}{s} + \frac{s}{\omega_d}\right), \tag{64}$$

$$\mathcal{C}_{lp}(s) = \frac{\omega_{lp}^2}{s^2 + 2\beta\omega_{lp}s + \omega_{lp}^2}, \tag{65}$$

$$\mathcal{C}_n(s) = \frac{\omega_p^2}{\omega_z^2} \cdot \frac{s^2 + 2\beta_z\omega_z s + \omega_z^2}{s^2 + 2\beta_p\omega_p s + \omega_p^2}. \tag{66}$$

For this case study, the design of a HIGS-based low-pass filter as presented in [23] is considered. Here, HIGS is added in series to the low-pass filter (65) together with an additional transfer function $\mathcal{C}_z(s) = \frac{s+\omega_c}{\omega_c}$ with $\omega_c = \frac{\omega_h}{k_h}|1 + \frac{4j}{\pi}|$. The linear portion of the controller is given by

$$\mathcal{C}(s) = \mathcal{C}_z(s)\mathcal{C}_{lp}(s)\mathcal{C}_{pid}(s)\mathcal{C}_n(s). \tag{67}$$

The system is subject to a bounded input disturbance $d \in \mathcal{L}_2$, and a unit step-input $r(t) = 1$ for $t \geq 0$, $r(t) = 0$ otherwise, which is approximated by the impulse response filter $\mathcal{U}_r(s) := \frac{1}{s+\epsilon}$, with $\epsilon = 10^{-6} > 0$ a small offset added for technical reasons, see [29] for a discussion on this well-known technicality in H_∞-control, and initial condition $x_r(0) = 1$. The specific closed-loop configuration is depicted in Fig. 7, and satisfies Assumption 1.

An initial controller is designed by means of a describing-function-based loop-shaping-like procedure, guided by an autotuner (see, *e.g.*, Section IV in [27]). Here, the aim is to maximize the bandwidth, *i.e.*, the frequency at which the quasi-linear open-loop frequency response function defined as $\mathcal{L}(j\omega) := \mathcal{P}(j\omega)\mathcal{C}(j\omega)\mathcal{D}(j\omega)$ crosses 0 dB for the first time, while satisfying a peaking constraint of 5 dB on the quasi-linear sensitivity function $\mathcal{S}(j\omega) := (1 + \mathcal{L}(j\omega))^{-1}$. The following parameter values are obtained: $k_p = 3.01 \cdot 10^7$ N/m, $\omega_i = 100 \cdot 2\pi$ rad/s, $\omega_d = 180 \cdot 2\pi$ rad/s, $\omega_{lp} = 1500 \cdot 2\pi$ rad/s, $\beta = 0.7$, $\omega_z = 1160 \cdot 2\pi$ rad/s, $\beta_z = 0.02$, $\omega_p = 850 \cdot 2\pi$, $\beta_p = 0.4$, $\omega_h = 270 \cdot 2\pi$ rad/s, $k_h = 1$, and the bandwidth is 250 Hz. A Nyquist-like plot of the quasi-linear open-loop frequency response function $\mathcal{L}(j\omega)$ is shown in Fig. 8. For the purpose of providing an intuitive feeling for the effect of the HIGS parameter ω_h on the closed-loop system behaviour, Fig. 8 additionally shows the quasi-linear open-loop frequency response function of two designs with $\omega_h = 150 \cdot 2\pi$ rad/s, and $\omega_h \to \infty$, of which the latter approaches the characteristics of a linear system. From a quasi-linear perspective, ω_h has a direct effect on the phase margin of the closed-loop system. Interestingly, this is in accordance with the time-domain step-response as depicted in Fig. 9. That is, an increase in the phase margin as predicted by the quasi-linear analysis leads to a reduction in overshoot, see also [24].

Remark 8. For the specific configuration as depicted in Fig. 7, the effect of choosing $k_h \neq 1$ can equivalently be regarded as a proportional scaling of both the output of HIGS as well as the parameter ω_h. Hence, one can lump the effect of choosing $k_h \neq 1$ into the proportional gain k_p of the linear part of the controller together with an appropriate scaling of ω_h, thereby allowing for the choice $k_h = 1$ without loss of generality. Note that, in this regard, the parameter k_h appears as a redundant parameter if used in conjunction with other control elements, which, therefore, renders the results for this specific example insensitive to a different choice for k_h.

5.2. Stability analysis

For verifying input-to-state stability of the resulting design, the conditions in Theorem 1 are solved without minimizing γ. The conservatism in the analysis is studied by varying the loop-gain k_p and HIGS parameter ω_h over a grid. The

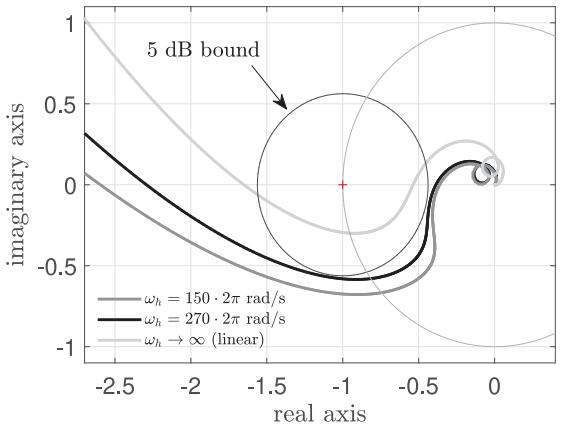

Fig. 8. Describing function based Nyquist plot of the open-loop frequency response function $\mathcal{L}(j\omega)$.

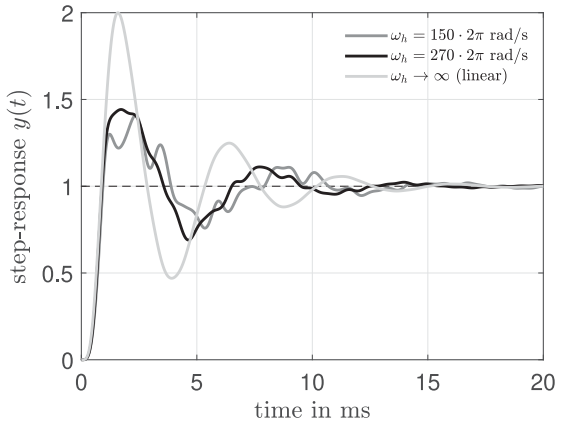

Fig. 9. Step-response for different values of ω_h.

remaining parameters are kept similar to the initial design. The choice for varying k_p and ω_h comes from the possibility to directly manipulate the gain margin through k_p and the phase margin through ω_h. The LMI-conditions are solved by means of the `MATLAB` toolbox `YALMIP` [45] together with the external solver `MOSEK` [46]. To improve overall numerical conditioning, a Gramian-based balancing of the closed-loop state-space realization is performed. Hereto, a similarity transformation $x_b = Tx$ is computed on the basis of the state-space description in integrator-mode, which is subsequently applied to both the integrator-mode and gain-mode state-space models for constructing a balanced closed-loop model. In order to demonstrate the relevance of Proposition 3, the LMIs in Theorem 1 are first solved with a two-dimensional partitioning (see [27, Section III]), and second with the more involved three-dimensional partitioning. The results are presented in Fig. 10. The stable region found by means of extensive time-series simulations is indicated by the grey area.

In Fig. 10(a), the conditions of Proposition 3 are violated in the region right to the dotted black line. As expected, with a two-dimensional partitioning no feasible solutions to the LMIs are found in that region. The benefits of a three-dimensional partitioning are clearly visible in Fig. 10(b) as feasible solutions are found beyond the dotted black curve. The results in Fig. 10(b) show a close correspondence between the results from Theorem 1 (LMIs) and the time-domain simulations, underlining the accuracy of the LMIs. In fact, the results seem to closely resemble what would be expected from a necessary condition for closed-loop stability of the nonlinear feedback system.

5.3. $\mathcal{L}_2$-gain

Next, the results of Theorem 1 are used for finding the smallest possible upper-bound on the $\mathcal{L}_2$-gain from an arbitrary input $d \in \mathcal{L}_2$ to the output e by minimizing γ. Compared to a linear controller, ω_h provides an additional degree of freedom in the HIGS-based controller and may thus be considered as an extra performance variable. It is therefore of interest to analyse the $\mathcal{L}_2$-gain for different values of ω_h. Note that in the analysis it is chosen to set $x_r(0) = 0$ so the reference $r = 0$. The results from solving the LMIs with a different number of regional partitionings are shown in Fig. 11.

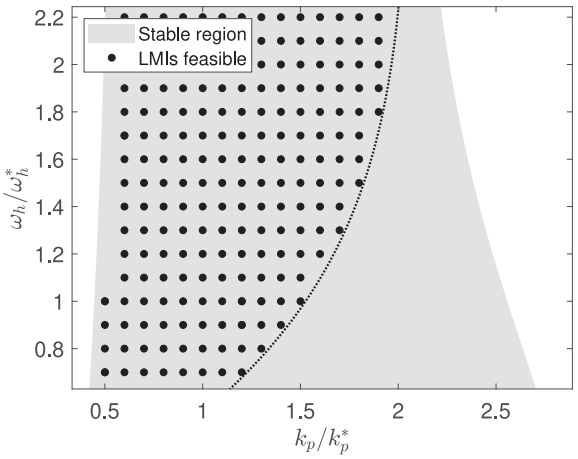

(a) Partitioning of the (z, u)-region.

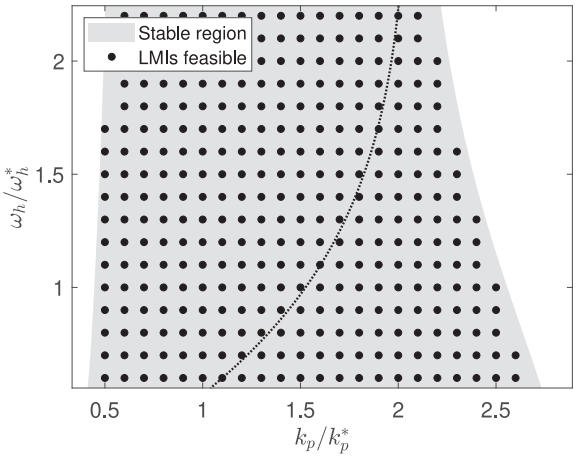

(b) Partitioning of the $(z, u, \dot{z})$-region.

Fig. 10. Stability of the closed-loop system evaluated on the basis of (i) the conditions in Theorem 1 (black dots) with different partitionings, and (ii) time-domain simulations (grey area). The results are shown in terms of dimensionless ratios, where $\omega_h^* = 270 \cdot 2\pi$ rad/s and $k_p^* = 3.01 \cdot 10^7$ N/m correspond to the initial design.

In addition, an estimate obtained from simulated experiments is provided. For this purpose, a truncated sinusoid defined by $d(t) = \sin(\omega t)$ for all $t \in [0, T]$ and $d(t) = 0$ otherwise, with $T = 10 \cdot 2\pi/\omega$ is applied to the closed-loop system at various frequencies. The simulation time is set to $T_f = 5 \cdot T$ s to ensure the response has sufficiently settled. A lower-bound on the $\mathcal{L}_2$-gain is then estimated by taking the maximum ratio of the computed input and output $\mathcal{L}_2$-norms.

The result in Fig. 11 clearly depicts the benefits of a partition refinement as the estimates become tighter and tighter. From Fig. 11, a closer correspondence between the results from Theorem 1 (LMIs) and the time-series simulations is observed for increasing values of ω_h. For decreasing values of ω_h, however, a clear discrepancy is visible. This may be caused by (i) remaining conservatism in the analysis, (ii) numerical artefacts, and (iii) the chosen class of input signals, which may only provide a lower-bound for the true $\mathcal{L}_2$-gain, that is, $\gamma_{\text{sim}} \leq \gamma \leq \gamma_{\text{LMI}}$.

5.4. $\mathcal{H}_2$-norm

Finally, the conditions presented in Theorem 2 are used for estimating the energy in the error response to a unit-step input approximated by $\mathcal{U}_r(s)$ with $x_r(0) = 1$. Again, ω_h is varied. As shown previously, increasing the phase margin in the quasi-linear design by varying ω_h translates to improved transient response as may be reflected in the $\mathcal{H}_2$-norm. No input disturbance is considered, *i.e.*, $d = 0$. The results of solving the LMIs for different partitionings are shown in Fig. 12, along with the $\mathcal{H}_2$-norm obtained from simulated time-series (grey). Note that, in contrast to the estimation of the $\mathcal{L}_2$-gain, the $\mathcal{H}_2$-norm obtained from simulations is exact.

Again Fig. 12 shows the benefits of a partition refinement, particularly for decreasing values of ω_h. For increasing values of ω_h, the LMI-results are in fair agreement with the true energy in the error response when the system is subject to a

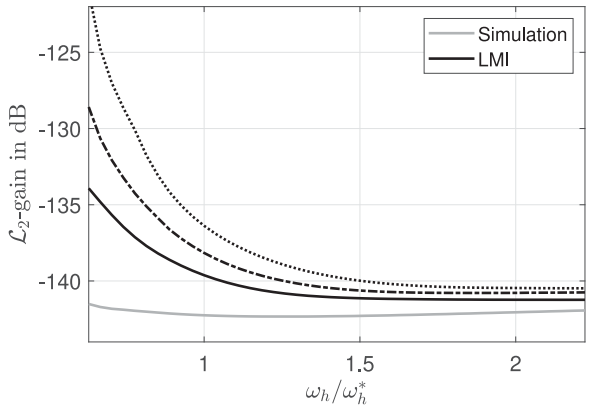

Fig. 11. Estimated $\mathcal{L}_2$-gain by means of (i) Theorem 1 with a different number of regional partitionings, $N = 3$ (·····), $N = 30$ (-·-·-·), and $N = 100$ (——), and (ii) time-domain simulations (grey) as a function of the dimensionless ratio ω_h/ω_h^* with $\omega_h^* = 270 \cdot 2\pi$ rad/s.

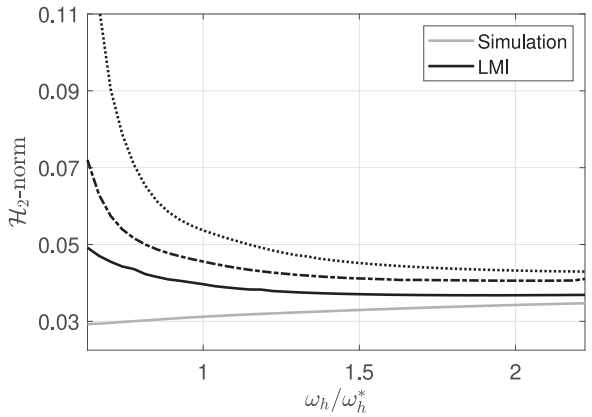

Fig. 12. Estimated $\mathcal{H}_2$-norm for a unit-step input on the basis of (i) Theorem 2 with a different number of regional partitionings, $N = 3$ (·····), $N = 30$ (-·-·-·), and $N = 100$ (——), and (ii) time-series simulations (grey) as a function of the dimensionless ratio ω_h/ω_h^* with $\omega_h^* = 270 \cdot 2\pi$ rad/s.

unit-step input. The difference between the simulations and LMI predictions may be caused by (i) remaining conservatism, and (ii) numerical artefacts/computational power. Note that the computational complexity significantly increases with an increasing number of regional partitions.

6. Conclusion

In this paper, rigorous conditions for stability and performance analysis of hybrid integrator–gain systems are presented. Two performance measures are considered: the $\mathcal{L}_2$-gain and the $\mathcal{H}_2$-norm. To potentially reduce conservatism in the analysis and obtain tighter performance estimates, flexible piecewise quadratic functions with a tailored and a numerically robust partition are proposed. In particular, for constructing such functions, the full region that determines mode-switching of HIGS is partitioned into smaller simplicial regions, each to which a quadratic Lyapunov-like function is assigned. The conditions are formulated as a convex optimization problem in terms of numerically verifiable LMIs. For achieving some more insight in feasibility of the LMIs with a regional partitioning, sufficient conditions are given under which the LMIs cannot be solved, guiding partition refinements which are important for obtaining accurate stability and performance estimates. The effectiveness of the presented tools has been demonstrated on a numerical example.

CRediT authorship contribution statement

Sebastiaan van den Eijnden: Conceptualization, Software, Writing – original draft. **W.P.M.H. Heemels:** Conceptualization, Supervision, Writing – review & editing. **Henk Nijmeijer:** Conceptualization, Supervision, Writing – review & editing. **Marcel Heertjes:** Conceptualization, Supervision, Writing – review & editing.

Declaration of competing interest

The authors declare that they have no known competing financial interests or personal relationships that could have appeared to influence the work reported in this paper.

References

[1] R.H. Middleton, Trade-offs in linear control system design, Automatica 27 (2) (1991) 281–292.
[2] J. Freudenberg, R. Middleton, A. Stefanopoulou, A survey of inherent design limitations, in: Proceedings of the American Control Conference, Vol. 5, 2000, pp. 2987–3001.
[3] O. Beker, C.V. Hollot, Y.Y. Chait, Plant with integrator: An example of reset control overcoming limitations of linear feedback, IEEE Trans. Autom. Control 46 (11) (2001).
[4] B. Hunnekens, N. van de Wouw, D. Nesic, Overcoming a fundamental time-domain performance limitation by nonlinear control, Automatica 67 (2016) 277–281.
[5] W. Foster, D. Gieseking, W. Waymeyer, A nonlinear filter for independent gain and phase (with applications), Trans. ASME J. Basic Eng. 78 (1966) 457–462.
[6] S. van Loon, B. Hunnekens, W. Heemels, N. van de Wouw, H. Nijmeijer, Split-path nonlinear integral control for transient performance improvement, Automatica 66 (2016) 262–270.
[7] J.P. Hespanha, A.S. Morse, Switching between stabilizing controllers, Automatica 38 (2002) 1905–1917.
[8] D. Liberzon, Switching in Systems and Control, Birkhauser, Boston, 2003.
[9] J.C. Clegg, A nonlinear integrator for servomechanisms, Trans. AIEE 77 (Part II) (1958) 41–42.
[10] C.V. Hollot, Y. Zheng, Y. Chait, Stability analysis for control systems with reset integrators, in: Proceedings of the 36th IEEE Conference on Decision and Control, 1997, pp. 1717–1719.
[11] O. Beker, C.V. Hollot, Y. Chait, H. Han, Fundamental properties of reset control systems, Automatica 40 (6) (2004) 905–915.
[12] D. Nesic, L. Zaccarian, A.R. Teel, Stability properties of reset systems, Automatica 44 (8) (2008) 2019–2026.
[13] Y. Chait, C.V. Hollot, On Horowitz's contributions to reset control, Internat. J. Robust Nonlinear Control 12 (2002) 335–355.
[14] W.H.T.M. Aangenent, G. Witvoet, W.P.M.H. Heemels, M.J.G. van de Molengraft, M. Steinbuch, Performance analysis of reset control systems, Int. J. Robust Nonlinear Control 20 (2009) 1213–1233.
[15] S.J.L.M. van Loon, K.G.J. Gruntjens, M.F. Heertjes, N. van de Wouw, W.P.M.H. Heemels, Frequency-domain tools for stability analysis of reset control systems, Automatica 82 (2017) 101–108.
[16] T. Loquen, D. Nesic, C. Prieur, S. Tarbouriech, A.R. Teel, L. Zaccarian, Piecewise quadratic Lyapunov functions for linear control systems with First Order Reset Elements, in: Proceedings of the IFAC Symposium on Nonlinear Control. Systems, 2010, pp. 807–812.
[17] Y. Guo, Y. Wang, L. Xie, Frequency-domain properties of reset systems with application in hard-disk-drive systems, IEEE Trans. Control Syst. Technol. 17 (2009) 1446–1453.
[18] L. Hazeleger, M. Heertjes, H. Nijmeijer, Second-order reset elements for stage control design, in: Proceedings of the American Control Conference, 2016, pp. 2643–2648.
[19] A. Palanikumar, N. Saikumar, S.H. HosseinNia, No more differentiator in PID: development of nonlinear lead for precision mechatronics, in: Proceedings of the ECC, Limassol, Cyprus, 2018, pp. 991–996.
[20] D.A. Deenen, M.F. Heertjes, W.P.M.H. Heemels, H. Nijmeijer, Hybrid integrator design for enhanced tracking in motion control, in: Proceedings of the American Control Conference, Seattle, Washington, USA, 2017, pp. 2863–2868.
[21] D.A. Deenen, B. Sharif, S.J.A.M. van den Eijnden, H. Nijmeijer, W.P.M.H. Heemels, M.F. Heertjes, Projection-based integrators for improved motion control: Formalization, well-posedness and stability of hybrid integrator-gain systems, Automatica (2020) in press.
[22] M.F. Heertjes, N. Irigoyen Perdiguero, D.A. Deenen, Robust control and data-driven tuning of a hybrid integrator-gain system with applications to wafer scanners, Internat. J. Adapt. Control Signal Process. (2018).
[23] S.J.A.M. van den Eijnden, Y. Knops, M.F. Heertjes, A hybrid integrator-gain based low-pass filter for nonlinear motion control, in: Proceedings of the Conference on Control Technology Applications, Copenhagen, Denmark, 2018, pp. 1108–1113.
[24] S.J.A.M. van den Eijnden, M.F. Heertjes, W.P.M.H. Heemels, H. Nijmeijer, Hybrid integrator-gain systems: A remedy for overshoot limitations in linear control? IEEE Control Syst. Lett. 4 (4) (2020) 1042–1047.
[25] M.K. Johansson, Piecewise Linear Control Systems: A Computational Approach, Springer-Verlag Berlin Heidelberg, 2003.
[26] M. Johansson, A. Rantzer, Computation of piecewise quadratic Lyapunov functions for hybrid systems, IEEE Trans. Automat. Control 43 (1998) 555–559.
[27] S.J.A.M. van den Eijnden, M.F. Heertjes, H. Nijmeijer, Robust stability and nonlinear loop-shaping design for hybrid integrator-gain-based control systems, in: American Control Conference (ACC), Philadelphia, PA, USA, 2019, pp. 3063–3068.
[28] J. Oehlerking, Decomposition of Stability Proofs for Hybrid Systems (Ph.D. thesis), Carl von Ossietzky University, Oldenburg, Germany, 2016.
[29] K. Zhou, J.C. Doyle, K. Glover, Robust and Optimal Control, Prentice Hall, New Jersey, 1996.
[30] S. Axler, K.A. Ribet, Topics in Hyperplane Arrangements, Polytopes and Box-Splines, Springer.
[31] R. Iervolino, F. Vasca, L. Iannelli, Cone-copositive piecewise quadratic Lyapunov functions for conewise linear systems, IEEE Trans. Automat. Control 60 (11) (2015).
[32] M. van de Wal, G. van Baars, F. Sperling, O. Bosgra, Multivariable H_∞/μ feedback control design for high-precision wafer stage motion, Control Eng. Pract. 10 (7) (2002) 739–755.
[33] B. Sharif, M.F. Heertjes, W.P.M.H. Heemels, Extended projected dynamical systems with applications to hybrid integrator-gain systems, in: Proceedings of the 58th IEEE Conference on Decision and Control, Nice, France, 2019, pp. 5773–5778.
[34] A. Gelb, W.E. Vander Velde, Multiple-Input Describing Functions and Nonlinear System Design, McGraw-Hill Book Company, 1968.
[35] W.P.M.H. Heemels, S. Weiland, Input-to-state stability and interconnections of discontinuous dynamical systems, Automatica 44 (2008) 3079–3086.
[36] C.A. Yfoulis, R. Shorten, A numerical technique for the stability analysis of linear switched systems, Internat. J. Control 77 (11) (2004) 1019–1039.
[37] R. Goebel, R.G. Sanfelice, A.R. Teel, Hybrid Dynamical Systems: Modeling, Stability and Robustness, Princeton University Press, 2012.
[38] J. Willems, Dissipative dynamical systems, Part I: General theory, Arch. Ration. Mech. Anal. 45 (5) (1972) 321–351.
[39] A. van der Schaft, $\mathcal{L}_2$-Gain and Passivity Techniques in Nonlinear Control, Springer, 2000.
[40] H.K. Khalil, Nonlinear Systems, Prentice Hall, Upper Saddle River, New Jersey, USA, 2002.
[41] S. Skogestad, I. Postlethwaite, Multivariable Feedback Control: Analysis and Design, John Wiley & Sons, New York, 2005.
[42] E. de Klerk, Aspects of Semidefinite Programming, Springer (US), 2002.
[43] D. Nesic, A. Teel, L. Zaccarian, Stability and performance of SISO control systems with first-order reset elements, IEEE Trans. Automat. Control 56 (2011) 2567–2582.

[44] M.K. Camlibel, W.P.M.H. Heemels, J.M. Schumacher, Stability and controllability of planar bimodal linear complementary systems, in: Conference on Decision and Control, Maui, Hawaii, USA, 2003, pp. 1651–1656.
[45] J. Lofberg, YALMIP: A toolbox for modeling and optimization in matlab, in: IEEE Int. Symp. on Computer Aided Contr. Sys. Design, Taipei, Taiwan, 2004, pp. 285–289.
[46] E.D. Andersen, C. Roos, T. Terlaky, On implementing a primal–dual interior-point method for conic quadratic optimization, Math. Program. 95 (2) (2003).